Article
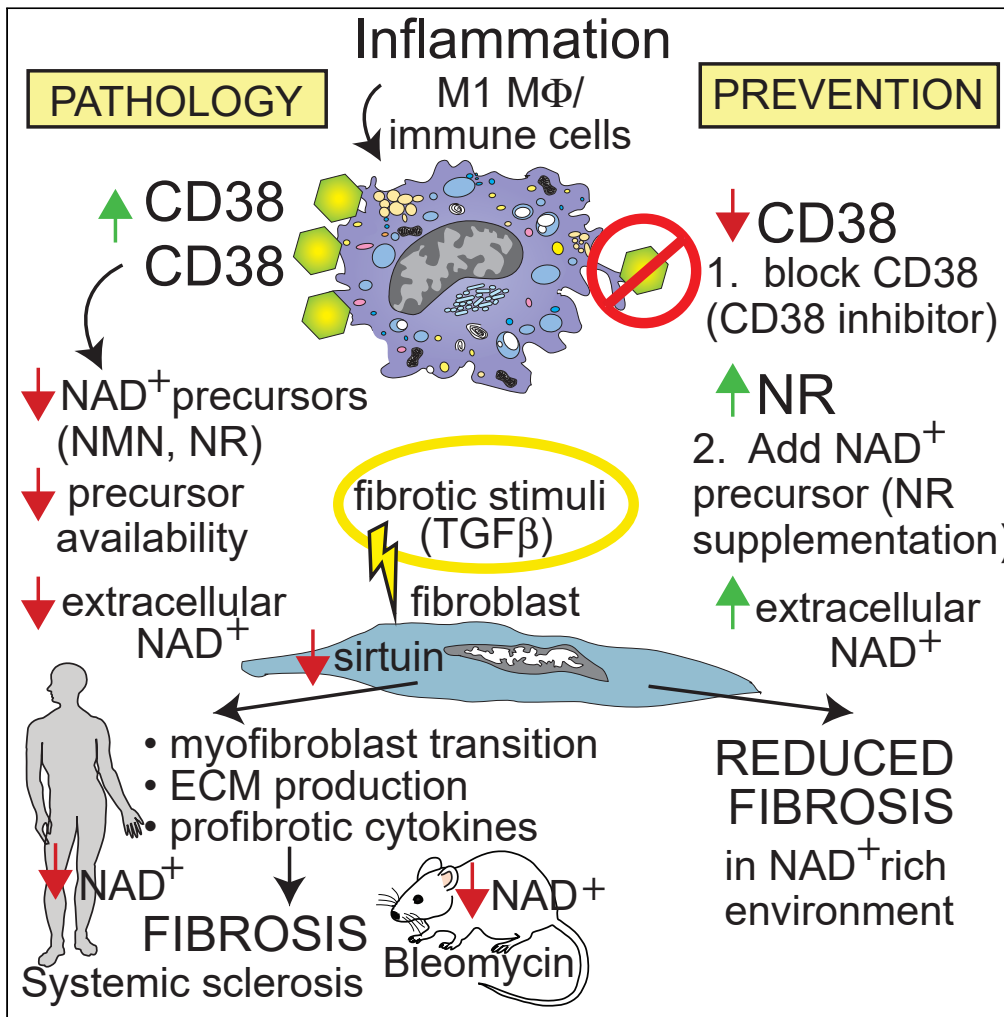
Targeting CD38-dependent NAD$^+$ metabolism to mitigate multiple organ fibrosis

Bo Shi, Wenxia Wang, Benjamin Korman, ..., Johann E. Gudjonsson, Eduardo N. Chini, John Varga

vargaj@umich.edu

HIGHLIGHTS

CD38 shows elevated expression in skin biopsies of patients with systemic sclerosis

Elevated CD38 is associated with reduced NAD$^+$ and augmented fibrotic responses

Genetic loss of CD38 is associated with increased NAD$^+$ levels and attenuated fibrosis

NAD$^+$ boosting via CD38 inhibition or NR supplementation prevents multi-organ fibrosis

iScience

Article

Targeting CD38-dependent NAD⁺ metabolism to mitigate multiple organ fibrosis

Bo Shi,[1] Wenxia Wang,[1] Benjamin Korman,[1] Li Kai,[1] Qianqian Wang,[1] Jun Wei,[1] Swarna Bale,[1] Roberta Goncalves Marangoni,[1] Swati Bhattacharyya,[1] Stephen Miller,[2] Dan Xu,[2] Mahzad Akbarpour,[3] Paul Cheresh,[3] Daniele Proccissi,[4] Demirkan Gursel,[5] Jair Machado Espindola-Netto,[7] Claudia C.S. Chini,[7] Guilherme C. de Oliveira,[7] Johann E. Gudjonsson,[6] Eduardo N. Chini,[7] and John Varga[1,8,9,*]

Summary

The processes underlying synchronous multiple organ fibrosis in systemic sclerosis (SSc) remain poorly understood. Age-related pathologies are associated with organismal decline in nicotinamide adenine dinucleotide (NAD⁺) that is due to dysregulation of NAD⁺ homeostasis and involves the NADase CD38. We now show that CD38 is upregulated in patients with diffuse cutaneous SSc, and CD38 levels in the skin associate with molecular fibrosis signatures, as well as clinical fibrosis scores, while expression of key NAD⁺-synthesizing enzymes is unaltered. Boosting NAD⁺ via genetic or pharmacological CD38 targeting or NAD⁺ precursor supplementation protected mice from skin, lung, and peritoneal fibrosis. In mechanistic experiments, CD38 was found to reduce NAD⁺ levels and sirtuin activity to augment cellular fibrotic responses, while inhibiting CD38 had the opposite effect. Thus, we identify CD38 upregulation and resulting disrupted NAD⁺ homeostasis as a fundamental mechanism driving fibrosis in SSc, suggesting that CD38 might represent a novel therapeutic target.

Introduction

Systemic sclerosis (SSc), a multisystem disease associated with high mortality, follows unpredictable clinical course and lacks effective therapy (Asano and Varga, 2019; Allanore et al., 2015). Gene expression profiling in SSc has uncovered deregulation of fibrotic and inflammatory/immune pathways, as well as patient-to-patient molecular heterogeneity (Franks et al., 2019). While the pathogenesis remains incompletely understood, a defining SSc hallmark is fibrosis that synchronously affects the skin and lungs and other internal organs (Varga and Abraham, 2007; Distler et al., 2019). Although the extent of fibrosis in SSc and its temporal trajectory are variable between individual patients and across affected organs, intractable fibrosis can lead to lethal organ failure (Bhattacharyya et al., 2011; Ho et al., 2014). Persistent tissue accumulation of myofibroblasts accounts for all forms of fibrosis (Hinz et al., 2012). Activated myofibroblasts originate from tissue-resident progenitors; however, the factors responsible for reprogramming these cells into activated myofibroblasts and of equal importance, preventing myofibroblast reversion toward a metabolically quiescent inactive state, remain largely unknown (Zhao et al., 2020). Thus, the development of effective anti-fibrotic therapies is predicated on comprehensive annotation of disease-specific mechanisms that positively or negatively regulate the differentiation, metabolism, and survival of profibrotic mesenchymal cells (Hinz and Lagares, 2020).

Sirtuins are nicotinamide adenine dinucleotide (NAD⁺)-dependent deacetylases best known for their fundamental roles in regulation of aging, health span, and longevity (Bonkowski and Sinclair, 2016). Recent studies uncovered an additional important role for sirtuins in regulating fibrotic responses, with suppression of collagen production and myofibroblast differentiation *in vivo* and *in vitro* (Wei et al., 2015; Akamata et al., 2016; Sosulski et al., 2017). Moreover, we and others have described impaired sirtuin expression and activity in fibrotic skin and lungs from patients with SSc, implicating sirtuin dysregulation in pathogenesis (Wei et al., 2015; Akamata et al., 2016; Sosulski et al., 2017; Zerr et al., 2016). However, the mechanisms underlying sirtuin dysregulation in patients with SSc are currently unknown. NAD⁺ is a cofactor for key metabolic processes and a substrate for sirtuins and other enzymes involved in cell signaling and damage repair (Yoshino et al., 2018; Chini et al., 2017). Recent studies have shown that levels of NAD⁺ as well as its

[1]Northwestern Scleroderma Program, Northwestern University Feinberg School of Medicine, Chicago, IL 60611, USA

[2]Department of Microbiology-Immunology, Northwestern University Feinberg School of Medicine, Chicago, IL 60611, USA

[3]Division of Pulmonary and Critical Care Medicine, Northwestern University Feinberg School of Medicine, Chicago, IL 60611, USA

[4]Department of Radiology, Northwestern University Feinberg School of Medicine, Chicago, IL 60611, USA

[5]Pathology Core Facility, Northwestern University Feinberg School of Medicine, Chicago, IL 60611, USA

[6]Department of Dermatology, University of Michigan, Ann Arbor, MI 48109, USA

[7]Department of Anesthesiology and Kogod Center on Aging, Mayo Clinic, Rochester 55905 MN, USA

[8]Department of Internal Medicine, University of Michigan, Ann Arbor, MI 48109, USA

[9]Lead contact

*Correspondence: vargaj@umich.edu

https://doi.org/10.1016/j.isci.2020.101902

precursors decline during natural aging, as well as in progeroid syndromes (Camacho-Pereira et al., 2016; Frederick et al., 2016; Gomes et al., 2013; Zhu et al., 2015; Tarrago et al., 2018). Notably, sirtuin activity is tightly regulated by NAD^+ bioavailability. Indeed, aging- and disease-associated decline in NAD^+ is accompanied by sirtuin dysfunction that contributes to pathogenesis (Guarente, 2011). The multifunctional NADase enzyme CD38 is a type II plasma membrane protein expressed on both immune and non-immune cells. CD38 shows ectoenzyme activity with the catalytic site facing the outside of the cell (De Flora et al., 1997; Boslett et al., 2018a; Chatterjee et al., 2018). CD38 is also present on intracellular organelles, including the nucleus and mitochondria (Sun et al., 2002; Aksoy et al., 2006a; Zhao et al., 2012; Peclat et al., 2020). As the main NAD^+-hydrolyzing enzyme in mammalian tissues, CD38 plays a key role in age-dependent decline in NAD^+ (Camacho-Pereira et al., 2016; Aksoy et al., 2006a, 2006b; Barbosa et al., 2007). Indeed, we showed that tissue levels and activity of CD38 are negatively correlated with NAD^+ levels during aging, and CD38 inhibition preserves tissue NAD^+ (Camacho-Pereira et al., 2016). The relative roles of CD38 extracellular versus the intracellular enzymatic activity in its biological effects have not been completely defined. However, in the majority of cells, CD38 is expressed mostly as an ecto-enzyme, a phenomenon known as the "topological paradox". Interestingly, recently we have demonstrated that in addition to controlling NAD^+ levels, CD38 also modulates the bioavailability of nicotinamide mononucleotide (NMN) and other extracellular precursors for intracellular NAD^+ biosynthesis, its activity governs organismal NAD^+ homeostasis (Camacho-Pereira et al., 2016).

We now show that CD38 is substantially elevated in the skin in patients with SSc, and levels are associated with both clinical disease severity and profibrotic signaling activity, while expression of key synthesizing enzymes in the NAD^+ salvage pathway are unaltered compared to healthy controls. Genetic and pharmacological targeting of CD38 raised NAD^+ levels, leading to attenuation of *in vitro* and *in vivo* fibrotic responses in explanted human skin fibroblasts and in preclinical disease models in mice, respectively. Similarly, boosting organismal NAD^+ via dietary supplementation with the precursor nicotinamide riboside (NR) prevented fibrosis in the skin, lungs, and peritoneal membrane. Thus, CD38 has a previously unrecognized pathogenic role in multiple organ fibrosis via dysregulation of NAD^+ homeostasis and sirtuin dysfunction. Targeting CD38-mediated NAD^+ metabolism might therefore represent a novel therapeutic approach to ameliorate chronic fibrosis.

Results

NAD^+-consuming enzymes are elevated in SSc

Cellular NAD^+ levels are tightly regulated via balanced NAD^+ degradation and production via *de novo* and salvage pathways (Canto et al., 2015; Yoshino et al., 2018; Chini et al., 2017). Dysregulated NAD^+ homeostasis, one of the hallmarks of biological aging, is accompanied by age-related metabolic and functional decline and a variety of pathologies in humans and in mice (Johnson and Imai, 2018; Chini et al., 2017). The decline in NAD^+ levels that occurs during aging has been shown to be due to changes in NAD^+ consumption and production. One of the key enzymes mediating age-related NAD^+ catabolism is the NADase CD38 (Camacho-Pereira et al., 2016). To determine if, similar to aging, SSc is also accompanied by altered expression of CD38 and other enzymes involved in maintaining NAD^+ homeostasis, we queried a transcriptome data set (GSE76886). Several cellular enzymes associated with either NAD^+ consumption or NAD^+ production showed differential mRNA expression in SSc skin biopsies, but only differences in expression of CD38, nicotinamide N-methyltransferase (NNMT), and IDO1 reached statistical significance (Figure 1B). In particular, CD38 mRNA was significantly elevated in skin biopsies from patients with SSc and diffuse cutaneous disease ($p < 0.0001$) but not with limited cutaneous disease ($p = 0.479$), with levels showing correlation with both clinical disease severity measured by the modified Rodnan skin score (MRSS), as well as with molecular markers of fibrosis (TGF-β and PDGF pathway scores) in the skin (Figures 1C–1E). In marked contrast, expression of CD38 showed negative correlation with SIRT1 pathway scores in the same skin biopsies (Figure 1F), consistent with compromised SIRT1 activity associated with CD38 upregulation. Significantly elevated tissue expression of CD38 in diffuse cutaneous SSc was confirmed by analysis of skin biopsy transcriptome data from two additional independent patient cohorts (Figure S1). The widely expressed cellular enzyme NNMT irreversibly methylates the NAD^+ precursor nicotinamide (NAM), thereby reducing its availability for NAD^+ salvage via the so-called NAM sink (Eckert et al., 2019; Pissios, 2017). Since upregulation of CD38 in SSc biopsies will generate NAM, which then serves as the substrate for NNMT in the NAD^+ clearance pathway (Figure 1A), it was notable that the combined gene score for these two NAD^+ consuming enzymes showed even more robust correlation with clinical skin scores and with the fibrotic TGF-β signature (Figure 1G). In contrast to upregulation of NAD^+-consuming enzymes observed in the
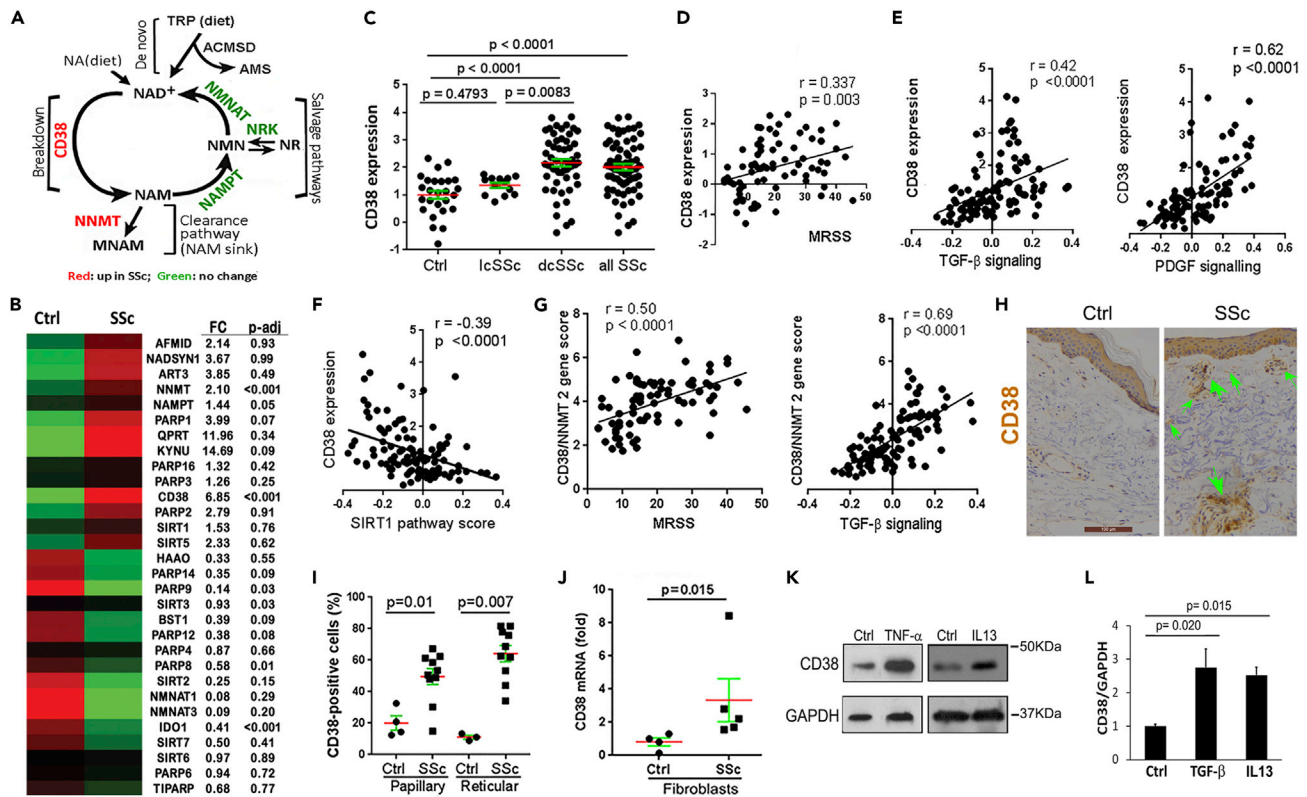
Figure 1. NAD$^+$-consuming enzyme CD38 significantly elevated in SSc skin biopsies

(A) Schematic of cellular NAD$^+$ metabolism, showing key enzymes catalyzing NAD$^+$ consumption and salvage.

(B) Heatmap indicating differential expression of key enzymes catalyzing NAD$^+$ consumption and salvage in healthy control (n = 26) and SSc (n = 68) skin biopsies (GSE76886, red indicates high and green indicates low expression).

(C) CD38 mRNA expression in healthy control and limited and diffuse cutaneous SSc (lcSSc and dcSSc) skin biopsies.

(D–F) Correlation of CD38 mRNA levels with modified Rodnan skin score (MRSS, range 0–51) and with TGF-β, PDGF, and SIRT1 pathway scores in the skin.

(G) Combined CD38 and NNMT gene score correlation with MRSS and with TGF-β signaling. Pearson's correlation.

(H) Immunohistochemistry of skin biopsies using antibodies to CD38; representative images. Arrows indicate CD38+ cells. Scale bar length represents 100 μm.

(I) Quantitation of CD38+ cells in the dermis; horizontal bars, means ± SEM (standard error of the mean) (10 SSc and 4 healthy control biopsies for (H) and (I), clinical data in Table S1 in Transparent Method).

(J) CD38 mRNA levels in explanted SSc (n = 5) and healthy control (n = 4) fibroblasts determined by qPCR.

(K and L) CD38 in human skin fibroblasts. Confluent cultures were incubated for 24 h with TNF-α (10 ng/mL), IL-13 (10 ng/mL), and TGF-β (10 ng/mL). (K) Whole cell lysates were analyzed by immunoblotting. (L) mRNA levels determined by qPCR, mean ± SEM. Experiments were repeated twice.

AMS: alpha-aminomuconate semialdehyde; ACMSD: aminocarboxymuconate semialdehyde decarboxylase; MNAM: N1-methylnicotinamide; NA: nicotinic acid; NAD: nicotinamide adenine dinucleotide; NAM: nicotinamide; NAMPT: nicotinamide phosphoribosyltransferase; NMN: nicotinamide mononucleotide; NMNAT: nicotinamide mononucleotide adenylyltransferase; NNMT: nicotinamide N-methyltransferase; NR: nicotinamide riboside; NRK: nicotinamide riboside kinase; TRP: tryptophan.

SSc skin biopsies, the principal NAD$^+$ salvage pathway enzymes (nicotinamide phosphoribosyltransferase [NAMPT], NMNAT1, and NMNAT3) (Yoshino et al., 2018; Chini et al., 2017) did not show differential expression, or were suppressed, in SSc (Figure S2A). Although the tissue expression level of NAD$^+$ metabolism genes does not necessarily predict their enzymatic activity, the present results nevertheless suggest that an imbalance in gene expression between NAD$^+$-producing and consuming enzymes might yield altered NAD$^+$ homeostasis in SSc.

We next generated a CD38 co-expression module defined as all genes (n = 194) showing correlation (Spearman r > 0.5) to CD38 in skin biopsies (GSE76886). Hierarchical clustering of skin biopsies using this 194-gene module as a classifier robustly separated the biopsies into two distinct clusters highly enriched for either healthy controls or SSc biopsies (chi-square p = 4.9*10^{-6}) (Figure S2B). To further evaluate CD38 expression in the skin, we immunostained skin biopsies from patients with SSc and healthy controls

(Table S1) using anti-CD38 antibodies. The numbers of CD38-immunopositive interstitial cells in the dermis were significantly elevated in SSc biopsies, with comparable increases noted in both the papillary and reticular dermal layers (Figures 1H and 1I). In explanted SSc skin fibroblasts (n = 5), CD38 mRNA levels were elevated compared to healthy matched control fibroblasts even after their serial *ex vivo* passages in culture (Figure 1J). Cellular expression of CD38 can be induced by a variety of soluble mediators (Hogan et al., 2019). Incubation of normal skin fibroblasts with TNF-α, IL-13, Toll-like receptor ligands, and TGF-β, each of which are implicated in SSc pathogenesis (Allanore et al., 2015), caused marked stimulation of CD38 expression (Figures 1K and 1L).

We next sought to characterize alterations in NAD^+ metabolism pathway enzymes in a bleomycin-induced mouse model of SSc characterized by inflammation and fibrosis in the skin, lung, and other organs (Yue et al., 2018). Interrogating a gene expression data set from bleomycin-treated mice (GSE71999) showed that CD38 mRNA expression was significantly elevated (p < 0.005) in fibrotic skin, and CD38 levels were correlated with NNMT levels (R^2 0.433, p = 0.004) (Figure S3A), while mRNA expression of NAD^+-synthesizing enzymes was comparable to that in untreated mice of the same age (Sargent et al., 2016). Upregulated expression of CD38 in fibrotic skin was confirmed in an independent mouse experiment (GSE 132869: Figure S3B). Subcutaneous bleomycin injection was accompanied by a substantial increase in $CD38^+$ cells in the lungs, with elevated CD38 expression noted on both peripherally derived CD45-positive leukocytes, as well as tissue-resident CD45-negative stromal cell populations (Figure S3C). In particular, we noted significantly increased numbers of CD38+ inflammatory monocytes, macrophages, plasmacytoid dendritic cells, and neutrophils in the lung from bleomycin-treated mice, whereas no change in B cells was seen (Figure S3D). Consistent with the putative functional linkage between enhanced NAD^+ consumption and fibrosis, bleomycin-treated mice demonstrated a significant drop in both circulating and tissue levels of NAD^+ (Figure S3E). Thus, fibrosis-associated upregulation of CD38 expression that is uncoupled from concomitant upregulation of NAD^+-producing enzymes will trigger pathogenic organismal NAD^+ depletion.

Deletion of CD38 ameliorated fibrosis

In view of the consistent coupling of skin fibrosis and increased CD38 expression observed both in patients with SSc as well as in preclinical disease models, together with reduced circulating and tissue NAD^+ levels in fibrotic mice, we sought to investigate the potential pathogenic role of CD38 by determining if targeting CD38 will mitigate fibrosis. For this purpose, we first characterized inducible fibrosis in CD38-null mice (Transparent Methods, Experimental Animals) at one year of age, when NAD^+ levels in wild-type mice show a significant decline (Figure 2A) (Camacho-Pereira et al., 2016). Absent CD38 expression in these mice was confirmed by immunoblot and flow cytometry in multiple tissues and cell types (Figure 2B). At baseline, the proportions of immune cell populations in the spleen were comparable in wild-type and CD38-null mice (data not shown). Bone-marrow-derived CD38-null macrophages showed unaltered *ex vivo* M1/M2 polarization; however, compared to wild-type M1 macrophages, CD38-null macrophages showed markedly impaired production of IL-6 and IL-1β (Figure 2C). These findings are consistent with previous reports documenting unaltered maturation and differentiation, but impaired function, of immune cells in CD38-null mice (Cockayne et al., 1998). One-year-old CD38-null mice showed 2- to 3-fold higher NAD^+ levels in multiple tissues (skin, lung, liver) compared to age-matched wild-type control mice (Figure 2D). CD38-null mice weighed less than wild-type mice of the same age, as reported previously (Chiang et al., 2015), but no overt behavioral or phenotypic differences were observed.

Chronic subcutaneous bleomycin administration in mice is a widely used approach to model SSc and fibrosis (Marangoni et al., 2016). In this model, bleomycin induces multiple organ fibrosis associated with both innate and adaptive immune response cells, including activation of CD4/8 T cells, B cells, and dendritic cells, thereby recapitulating the principal inflammatory-fibrotic processes that characterize SSc (Allanore et al., 2015). Remarkably, CD38-null mice showed attenuation of the bleomycin-induced fibrotic process, including increase in dermal thickness and collagen accumulation (Figure 2E). Notably, weight loss sustained during the course of bleomycin treatment was significantly attenuated in CD38-null mice (Figure 2F). Furthermore, lungs from CD38-null mice treated with bleomycin also showed that the severity of radiologic and histological fibrosis significantly ameliorated, albeit not fully abrogated (Figures 2G and 2H). Attenuation of fibrosis was accompanied by reduced collagen accumulation and expression of fibrotic genes COL1A1 and COL3A1, as well as the alternately spliced extracellular matrix components
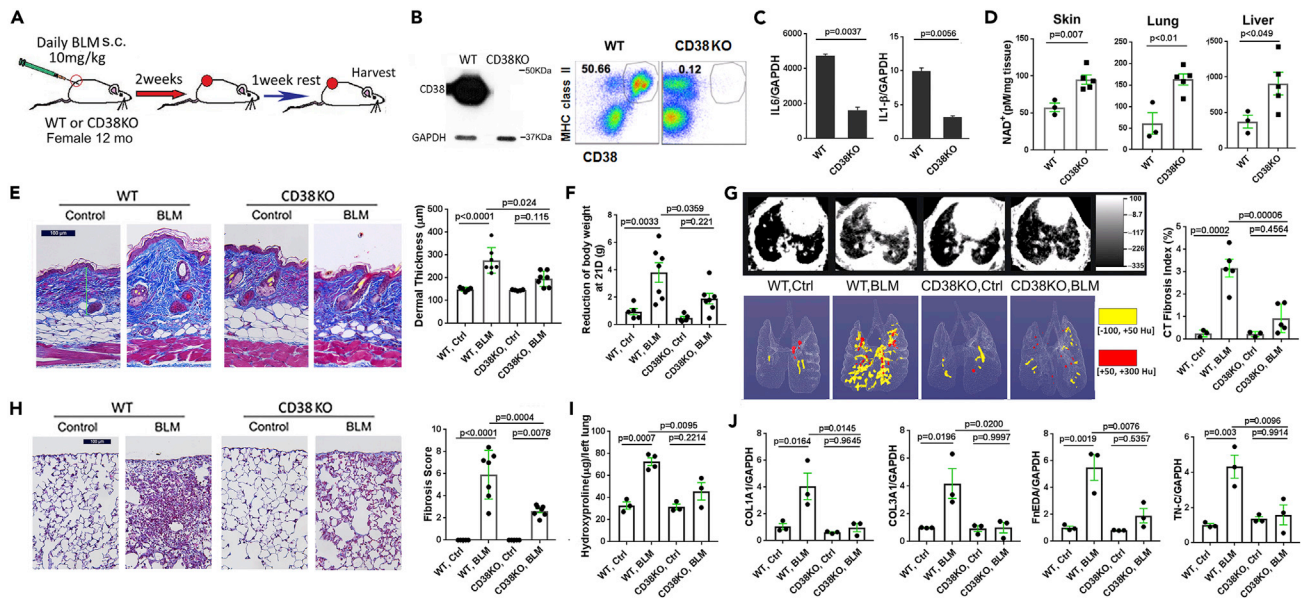
Figure 2. Deletion of CD38 ameliorated skin and lung fibrosis

(A) Schematic of experimental design. Twelve-month-old female CD38-null mice or wild-type control mice on standard chow received daily s.c. bleomycin (BLM) injections (10 mg/kg) for 14 d. After 21 d, mice were sacrificed. Five to 7 mice were used for each group, and experiments were repeated 2 times.

(B) CD38 expression undetectable in inguinal lymph nodes (representative immunoblot) and spleen cells (flow cytometry) in CD38-null mice.

(C) Reduced cytokine gene expression (qPCR) in CD38-null bone-marrow-derived M1 macrophages.

(D) Elevated NAD$^+$ levels in skin, lungs, and liver in CD38-null mice.

(E) Attenuated increase in dermal thickness (representative images, trichrome stain; scale bar represents 100 μm) and collagen deposition in CD38-null mice. Results are means $\pm$ SEM (standard error of the mean) from an experiment representative of two independent experiments.

(F) Bleomycin treatment-induced weight loss is mitigated in CD38-null mice (n = 5–7 mice/per group).

(G–J) Lung fibrosis induced by bleomycin is attenuated in CD38-null mice. (G) microCT of the lungs (n = 5 mice/group). Representative cross-sectional and 3D images (left) and quantitative lung fibrosis index (right). (H) Lung histology (trichrome stain, scale bar represents 100 μm); representative images (left) and measurement of lung fibrosis (right). (I and J) Collagen accumulation and fibrotic gene expression in the lungs. Error bars in all graphs, means $\pm$ SEM.

---

fibronectin-EDA and tenascin-C, recognized markers of fibrosis that are abundantly expressed in the fibrotic tissue in SSc (Figures 2I and 2J) (Van Der Straaten et al., 2004; Bhattacharyya et al., 2014, 2016).

NAD$^+$ boosting ameliorated skin and lung fibrosis in mice

In view of the substantial fibrosis protection accompanied by a rise of NAD$^+$ levels that was noted in mice lacking CD38, the principal NAD$^+$-consuming enzyme, we sought to determine if organismal NAD$^+$ boosting by either selectively blocking its CD38-mediated hydrolysis and/or by NAD$^+$ precursor supplementation will mitigate fibrosis. To this end, 18-month-old female mice maintained for 2 weeks on either standard chow diet or chow supplemented with nicotinamide riboside (NR, 3 g/kg chow) were treated with a thiazoloquin(az)olin(on)e compound 78c selective for the CD38 NADase (Tarrago et al., 2018). Treatment with 78c (30 mg/kg weight) administered by daily oral gavage was initiated concomitantly with a two-week course of daily subcutaneous bleomycin injections, and mice remained on NR-supplemented chow diet and continued daily 78c gavage until sacrifice at day 21 (Figure 3A). On standard chow diet, mice treated with bleomycin suffered significant weight loss (maximal 40% at day 11), which however was substantially attenuated in mice on an NR-supplemented chow diet combined with the CD38 inhibitor 78c (Figure 3B). Dietary NR supplementation by itself, or combined with 78c treatment, resulted in a ~5-fold increase in skin NAD$^+$ levels compared to mice treated with bleomycin only (Figure 3E). Notably, boosting NAD$^+$ in bleomycin-treated mice resulted in significantly improved skin fibrosis, including attenuated increase in dermal thickness, skin collagen content, and fibrotic gene expression, as well as the number of ASMA (alpha smooth muscle actin)-positive myofibroblasts in the lesional dermis (Figures 3C, 3D, 3F, 3G, S4A and S4B). In the skin, the anti-fibrotic efficacy of supplementation with NR was greater compared to the efficacy of CD38 inhibitor treatment. This differential response might reflect limited tissue penetration of the CD38 inhibitor. The expansion of the fibrotic dermis was inversely correlated with tissue levels of NAD$^+$, directly linking NAD$^+$ boosting in the anti-fibrotic effect (Figure 3E). Strikingly, NAD$^+$ boosting by either NR
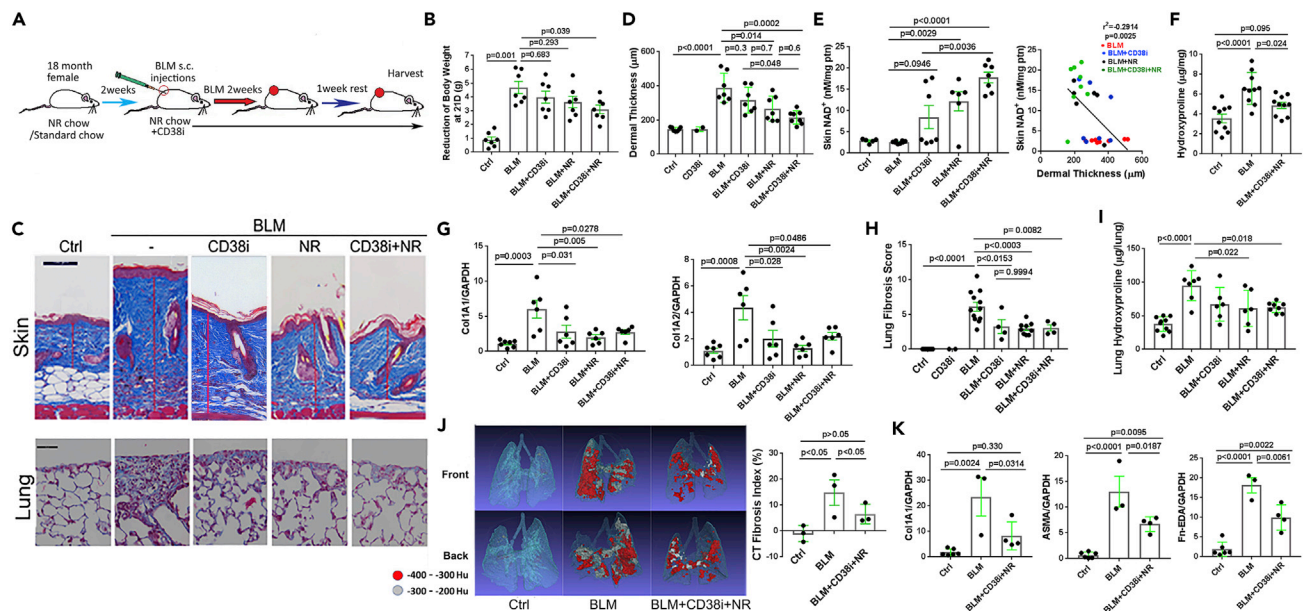
Figure 3. NAD$^+$ boosting ameliorated skin and lung fibrosis in aged mice

(A) Schematic of experimental design. Eighteen-month-old female C57/BL6 mice maintained on standard chow or NAD precursor nicotinamide riboside (NR)-supplemented chow diet. Mice received daily s.c. bleomycin (BLM) injections for 14 d alone or combined with CD38 inhibitor 78c administered by oral gavage. At 21 d, mice were sacrificed and skin and lungs were harvested for analysis. Results from three independent experiments with 6–8 mice per group.

(B–D) NAD$^+$ boosting attenuated bleomycin-induced (B) body weight loss, and (C and D) increase in dermal thickness (representative images, trichrome stain; scale bars represent 100 μm). Results are means ± SEM (standard error of the mean) from an experiment representative of three independent experiments.

(E) NAD$^+$ levels in the skin; results are means ± SEM; negative correlation (Pearson's) of skin NAD$^+$ levels with dermal thickness.

(F–H) (F and G) Skin collagen content (hydroxyproline assays); and gene expression (qPCR); (C) (H) Lung fibrosis quantification (modified Ashcroft score).

(I) Lung collagen content.

(J) Lung fibrosis imaging, representative microCT images (left) and fibrosis quantitation (right).

(K) mRNA levels in the lung determined by qPCR; results are means ± SEM.

supplementation or via CD38 inhibition also afforded mice robust protection from pulmonary fibrosis, with significantly ameliorated radiological and histological fibrotic changes in the lungs coupled with reduced collagen accumulation and fibrotic gene expression (Figures 3C and 3H–3K). Monocytes and macrophages are thought to play an important role in the pathogenesis of organ fibrosis in SSc and in mouse models of the disease (Bhandari et al., 2020; Marangoni et al., 2016). Significant accumulation of macrophages in both the dermis and the lungs from bleomycin-treated mice was mitigated with NAD$^+$ boosting via treatment of mice with CD38 inhibitor or NR supplementation alone or in combination (Figure S5A and S5B). In particular, the combination treatment markedly attenuated the accumulation of CD11b + macrophages in the skin (Figure S5C) and CD64$^+$CD11b$^+$Siglec^{low} (myeloid derived) infiltrating macrophages in the lung, while having no significant effect on CD64$^+$CD11b$^+$Siglec^{high} (tissue resident) macrophages (Figure S5D). In view of the pivotal role that macrophages and other myeloid-derived leukocytes play in SSc pathogenesis (Bhandari et al., 2020), the decrease in macrophage accumulation observed in mice with NAD$^+$ boosting might contribute to the anti-fibrotic effect of this intervention.

Next, we examined how genetic or pharmacological CD38 targeting will modulate the development of the peritoneal membrane fibrosis induced by i.p. chlorhexidine gluconate (CG) injections (Bhattacharyya et al., 2018). Since this inducible model reproduces many fundamental processes underlying the pathogenesis of SSc, including inflammation, myofibroblast accumulation, and extracellular matrix accumulation, it is used widely to investigate pathogenic mechanisms of fibrosis (Costalonga et al., 2020; Kitamura et al., 2015). Mice lacking CD38 suffered less weight loss during the course of CG treatment and showed significantly attenuated peritoneal membrane thickening and collagen deposition (Figures S6A and S6B). Moreover, accumulation of myofibroblasts in the fibrotic peritoneal membrane was also dramatically attenuated in mice lacking CD38 (Figure S6C). Comparable protection from CG-induced peritoneal fibrosis was seen when wild-type mice were treated with the combination of NR plus CD38 inhibitor (Figure S6). Together,

these results further highlight the fundamental role of CD38 in governing the intensity of fibrotic processes in multiple organs.

CD38 and NAD$^+$ metabolisms govern cellular fibrotic responses

To investigate how CD38 governs profibrotic cellular responses at a mechanistic level, a series of experiments with explanted human and mouse cells were performed. In order to experimentally recapitulate cellular CD38's outward-facing enzyme function in the *in vivo* milieu (Tarrago et al., 2018; Hogan et al., 2019), we incubated quiescent skin fibroblasts at confluence with recombinant human CD38. CD38 augmented the profibrotic effects of TGF-β, with increased COL1A1 and ASMA mRNA expression, collagen production, and myofibroblast differentiation, which were accompanied by increased lysine acetylation, an established marker for sirtuin activity (Figures 4A and 4B). In contrast, supplementing fibroblast cultures with NR led to a significant rise in cellular NAD$^+$ levels that was accompanied by attenuation of TGF-β-induced profibrotic responses including stimulation of ASMA and COL1A1 gene expression (Figures 4C–4E). Likewise, incubation of human skin fibroblasts with 78c, which selectively inhibits CD38 NADase activity, suppressed basal collagen gene expression and ASMA levels and prevented their stimulation by TGF-β (Figures 4F and 4H). Moreover, skin fibroblasts explanted from CD38-null mice failed to respond to profibrotic TGF-β stimulation (Figure 4I). In contrast, pharmacological blockade of the cellular NAD$^+$ salvage pathway using the NAMPT inhibitor FK866 resulted in enhanced fibrotic gene expression, coupled to enhanced acetylation of cellular lysines and MnSOD, confirming a reduction in sirtuin activity (Figures 4J and 4K).

To examine the impact of CD38 blockade on sirtuin activity, we used bone-marrow-derived macrophages, which show inducible expression of endogenous CD38 upon LPS treatment (Camacho-Pereira et al., 2016). In LPS (lipopolysaccharides)-treated CD38+ macrophages, NAD$^+$ boosting 78c treatment resulted in increased sirtuin, as demonstrated by decreased levels of acetylated lysine (Figure 4G). Sirtuin activation itself had been previously implicated in suppression of fibrotic responses (Wei et al., 2015; Akamata et al., 2016). To further investigate the cellular mechanisms involved in the anti-fibrotic effects of NAD$^+$ boosting, we examined the effect of NR supplementation on mediators of profibrotic cellular fibrotic responses, focusing on the histone acetyltransferase p300 and Smad2. We had shown previously that p300 is a TGF-β-inducible cofactor that is indispensable for Smad-dependent cellular responses and is implicated in SSc pathogenesis (Ghosh et al., 2013; Ghosh and Varga, 2007). Significantly, NR supplementation of fibroblasts prevented the induction of p300 by TGF-β (Figure 4L). Additionally, Smad2 phosphorylation and nuclear translocation, which are induced by TGF-β to mediate its profibrotic effects (Mori et al., 2004), were markedly reduced by NR supplementation, as well as by CD38 inhibition (Figure 4M). Moreover, NR plus CD38 inhibition attenuated, although failed to completely prevent, fibroblast differentiation into myofibroblasts (Figure 4M and 4N). Induction of Smad-dependent transcriptional activity by TGF-β was only partially reduced by NR (Figure 4O). These results together demonstrate that negative and positive modulation of cellular NAD$^+$ homeostasis in fibroblasts via orthogonal loss-of-function and gain-of-function approaches profoundly influence myofibroblast activation, profibrotic cellular signaling, and regulation of fibrotic gene expression.

Discussion

The present results demonstrate that SSc, the prototypic multisystem fibrotic disease, is associated with elevated expression of the NAD$^+$-consuming enzyme CD38 in the absence of parallel increase in NAD$^+$ salvage pathway enzymes, with CD38 levels correlating with both clinical disease severity and with fibrotic signal activity in the skin. Similar alterations in tissue CD38 seen in a mouse model of scleroderma were accompanied by significant reduction in systemic NAD$^+$, reflecting a conserved linkage between disrupted NAD$^+$ homeostasis and fibrosis in both SSc and in mouse models of disease. Blocking CD38 *in vivo* via either genetic targeting or treatment with a selective NADase inhibitor alone or combined with NAD$^+$ precursor supplementation resulted in boosting NAD$^+$ levels and reduced fibrosis propensity in multiple organs. Fibrotic responses were also attenuated in explanted fibroblasts lacking CD38. Similarly, boosting NAD$^+$ via precursor supplementation of fibroblast cultures attenuated the magnitude of inducible fibrotic cellular responses via increased sirtuin activity and disruption of Smad-dependent canonical TGF-β signaling, while in contrast, ectopic CD38 augmented these fibrotic responses. Together, these observations uncover a previously unsuspected fundamental role for CD38-mediated NAD$^+$ metabolism in SSc fibrosis.
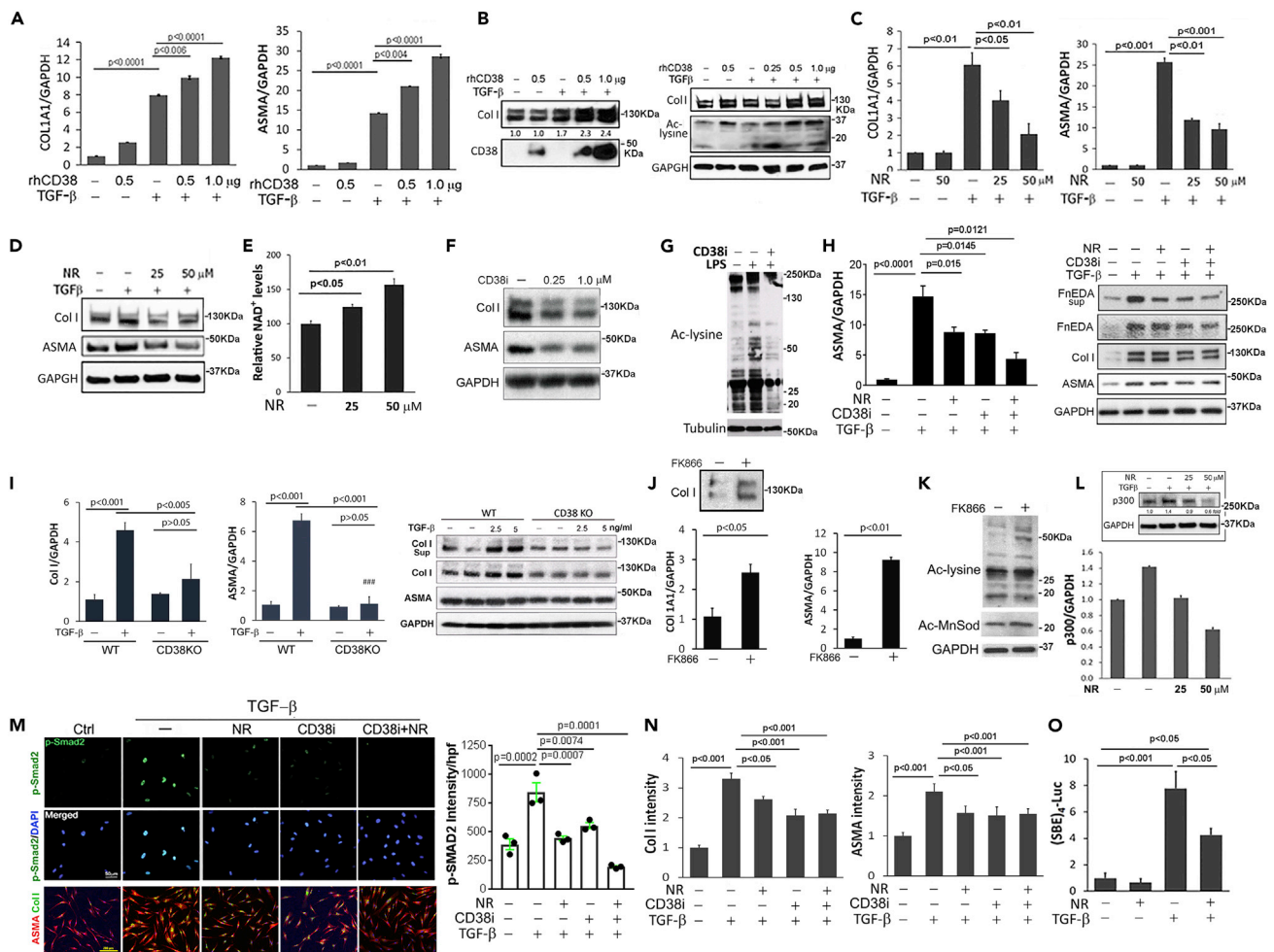
Figure 4. CD38 and NAD⁺ levels govern fibrotic cellular responses

Confluent foreskin fibroblasts (all except [G] and [I]) or CD38-null mouse fibroblasts (I) were incubated with TGF-β1 (10 ng/mL) in the presence or absence of recombinant human CD38 (rhCD38), 78c CD38 inhibitor (CD38i, 1 μM), FK866 (10 nM), and NR (50 μM or indicated concentrations).

(A) Levels of COL1A1 and ASMA mRNA determined by qPCR.

(B) Collagen production and sirtuin activity determined by immunoblot.

(C–E) (L) NR supplementation reduced collagen and ASMA stimulation, increased cellular NAD⁺ levels (E), and mitigated stimulation of p300 (L).

(F and I) Collagen and ASMA levels in wild-type and CD38-null mouse fibroblasts detected by immunoblotting and qPCR.

(G) Mouse bone-marrow-derived macrophages were *ex vivo* differentiated and incubated with LPS to induce endogenous CD38, followed by treatment with CD38i. Levels of lysine acetylation, a validated marker of sirtuin activity, were determined; representative immunoblot.

(H) CD38 inhibitor 78c and NR reduce levels of collagen, ASMA, and Fn-EDA.

(J and K) Incubation with FK866 (NAMPT inhibitor); effects on gene expression and lysine acetylation detected by qPCR and immunoblot.

(M and N) CD38 inhibition and NR mitigated myofibroblast transformation (confocal microscopy), fibrotic gene expression, and Smad2 phosphorylation and nuclear translocation (immunoblot).

(O) NR supplementation reduced Smad-dependent transcriptional activity in transiently transfected fibroblasts.

Experiments were performed in triplicate and repeated three times ([C] [D] [F] [K] [L]) or twice ([A] [B] [M] [N] [O]). Error bars in all graphs, means ± SEM (standard error of the mean).

Ample evidence supports the autoimmune nature of SSc, with dysregulated humoral and cellular immunity, both of which prominently contribute to disease pathogenesis (Allanore et al., 2015). Similar to normal wound healing, SSc has an early inflammatory phase where leukocyte-derived mediators trigger fibroblast activation and differentiation into myofibroblasts (Distler et al., 2019; Hinz and Lagares, 2020). In contrast to physiologic self-limited tissue repair, however, unresolving fibrosis in SSc is associated with durable myofibroblast activation and persistence resulting from combination of cell-autonomous metabolic and epigenetic changes coupled with structural and biochemical alterations in the tissue microenvironment. We now

demonstrate that the multifunctional NADase CD38 was significantly elevated in skin biopsies from multiple independent SSc patient cohorts. Described originally as a surface marker of activated T cells, CD38 is in fact broadly expressed on lymphoid and myeloid immune cells, as well as stromal cells including endothelial cells and fibroblasts (Reinherz et al., 1979; Malavasi et al., 2008; Tarrago et al., 2018). A principal enzymatic activity of CD38 is NAD^+ hydrolysis, which accounts for the key roles of CD38 in several physiologic and disease processes including inflammation, cancer, and metabolic diseases (Barbosa et al., 2007; Malavasi et al., 2008; Chini et al., 2018). Moreover, it is increasingly recognized that decline in NAD^+ levels that accompanies chronological aging in both humans and rodents is a key factor underlying the development of frailty and age-related metabolic and health decline (Zhu et al., 2015; Braidy et al., 2011; Massudi et al., 2012; Clement et al., 2019; Tarrago et al., 2018; Camacho-Pereira et al., 2016). Notably, CD38 appears to be the enzyme largely responsible for the organismal NAD^+ decline and resultant sirtuin dysfunction that characterize aging (Camacho-Pereira et al., 2016).

Originally identified on immune cells as a cell surface marker, CD38 is a widely expressed multifunctional enzyme that catalyzes the cleavage of a β-glycoside bond between nicotinamide and the ribose moiety of NAD^+, with the majority of NADase activity generating nicotinamide (Chini et al., 2018). The cellular localization of CD38 is unusual, with a majority showing a type II membrane orientation with the catalytic site facing the outside of the cell (Da Silva et al., 1998). However, CD38 is also present on intracellular organelles and has endoenzyme activity. The apparent "topological paradox" of CD38 ectoenzyme activity regulating NAD^+ homeostasis since NAD^+ is predominantly intracellular was recently shown to be attributable, at least, in part, to CD38 regulation of the extracellular levels of NMN as a precursor for intracellular NAD^+ synthesis (Chini et al., 2020; Camacho-Pereira et al., 2016; Shrimp et al., 2014; Tarrago et al., 2018). Via these catalytic processes, CD38 regulates organismal NAD^+ homeostasis and plays a fundamental role in determining the activity of multiple sirtuins along with other NAD^+-dependent cellular processes (Aksoy et al., 2006b). In the heart, CD38 expression on both endothelial cells and fibroblasts showed marked induction following ischemia reperfusion injury, and treatment with CD38 inhibitor had a strong cardio-protective effect associated with reversal of NAD^+ decline (Reyes et al., 2015; Boslett et al., 2018a, 2018b, 2019). We recently demonstrated upregulated CD38 expression and activity in aging mice and showed that CD38 is largely responsible for age-dependent organismic decline in NAD^+ levels (Camacho-Pereira et al., 2016). Both genetic targeting of CD38, as well as treatment with a selective thiazoloquin(az)olin(on)e CD38 inhibitor, reversed age-related NAD^+ decline, rescued sirtuin activity, and ameliorated multiple physiological and metabolic parameters of aging, including frailty, declining muscle and cardiac function, and exercise capacity, in mouse models of natural and accelerated aging (Tarrago et al., 2018). We now demonstrate that CD38 expression is elevated in SSc skin biopsies compared to that of healthy controls in a manner analogous to CD38 upregulation seen in aging mice and show that genetic and pharmacological NAD^+ boosting has salutary anti-fibrotic effects in mouse models. These observations draw attention to intriguing parallels between the biology of aging and SSc fibrosis attributable to CD38-dependent dysregulation of NAD^+ homeostasis.

In human skin, CD38 is detected primarily on T cells, myeloid cells, pericytes, and plasma cells (Tabib et al., 2018). The expression of CD38 is positively regulated in a variety of cell types by inflammatory and profibrotic cytokines, including IL-13, TGF-β, and IL-6, along with the senescence-associated secretory pattern. These extracellular cues, via NF-κB- and STAT-mediated intracellular signaling, induce CD38 expression to reduce NAD^+ levels (Chini et al., 2018, 2019). Analysis of transcriptome data sets showed increased levels of CD38 in skin biopsies from multiple independent SSc patient cohorts and positive correlation between CD38 expression in the skin and clinical measures and molecular markers of fibrosis. However, whether it is the action IL-6 or other secreted factors that lead to elevated CD38 expression in patients with SSc, and the cell types in the skin that are primarily responsible remain to be established. We had shown previously that the functional and metabolic decline that accompany aging are attenuated in CD38-null mice (Tarrago et al., 2018). We now demonstrate that CD38-null mice were also substantially protected from fibrosis in the skin, lung, and peritoneal lining membrane. Moreover, treatment of aged mice with the selective and potent CD38 NADase inhibitor 78c markedly reduced tissue accumulation of CD38+ inflammatory cells, reversed NAD^+ decline, and substantially ameliorated fibrotic and inflammatory changes, while genetic and pharmacological modulation of NAD^+ metabolism *ex vivo* in cultured fibroblasts elicited marked effects on the transcriptional regulation of fibrotic responses. Whether the anti-fibrotic effect of CD38 inhibition we observed in distinct fibrosis models is due primarily to reduced tissue accumulation of macrophages and inflammatory cells, or to a direct anti-fibrotic activity, remains to be conclusively established. Association of disrupted

NAD$^+$ homeostasis with altered tissue repair, extracellular matrix remodeling, and fibrosis has been previously recognized, albeit the experimental support coming primarily from animal models (Peclat et al., 2020). For instance, NAD$^+$ boosting via dietary NR supplementation was shown to ameliorate fibrosis of the skeletal muscle and heart in *mdx* mice (Ryu et al., 2016) and fibrosis of the liver (Zhou et al., 2016; Pham et al., 2019). An alternate NAD$^+$ boosting strategy using NMN supplementation was shown to similarly ameliorate fibrosis in the lung induced by intratracheal bleomycin (Liu et al., 2020). Moreover, we had previously shown that spontaneous fibrosis of the skeletal muscle in aging mice is associated with NAD$^+$ depletion and impaired sirtuin activity and can be mitigated by treatment with the NADase inhibitor 78c (Tarrago et al., 2018). These observations, taken together with the present results in mouse models of fibrosis induced by subcutaneous bleomycin or intraperitoneal chlorhexidine gluconate treatment, further strengthen the link between NAD$^+$ dysregulation and fibrosis and provide compelling support for the potential of NAD$^+$ boosting as a novel therapeutic strategy to prevent, slow the progression, or promoter regression, of fibrosis. These observations notwithstanding, it remains conceivable that CD38 elevation observed in the SSc skin biopsies and in lesional tissue from bleomycin-treated mice in the present report contribute to fibrosis pathogenesis in these conditions through alternate mechanisms that are independent of NAD$^+$ consumption and depletion. These alternate pathogenic mechanisms linking CD38 and fibrosis merit further investigation.

In summary, we demonstrate that in patients with SSc, as well as in preclinical disease models in mice, fibrosis is associated with upregulation of NAD$^+$-consuming enzymes in the absence of concomitant elevated NAD$^+$ production, leading to dysregulated NAD$^+$ homeostasis. Consequent decline in NAD$^+$ levels and functional impairment of sirtuins and other NAD$^+$-dependent metabolic enzymes contributes directly to myofibroblast transition that underlies intractable fibrosis in SSc. Boosting NAD$^+$ levels via genetic or pharmacological CD38 targeting, or via NAD$^+$ precursor supplementation, mitigated multiple organ fibrosis in rodent models and in explanted fibroblasts, at least in part by augmenting sirtuin activity and disrupting Smad-dependent core profibrotic TGF-β signaling. Thus, pharmacological approaches to boost organismal NAD$^+$ via inhibiting CD38 activity, by NAD$^+$ precursor supplementation or by a combination of both, represent potential therapeutic strategies for slowing or reversing fibrosis in SSc.

Limitations of the study

We acknowledge some limitations to our study. First, while we demonstrate elevated expression of the NAD$^+$ consuming enzyme CD38 in the skin biopsies from multiple independent SSc patient cohorts, raising the possibility that CD38 upregulation leads to enhanced NAD$^+$ catabolism and consequent decline in tissue NAD$^+$ bioavailability, we have not provided direct evidence of reduced NAD$^+$ levels in these biopsies. Additional studies will therefore measure levels of NAD$^+$, along with its precursors and metabolites, in both tissue and circulation from patients with SSc and age-matched healthy controls. Second, the present studies do not clearly delineate the principal cell types in the skin responsible for elevated CD38 expression in SSc biopsies. Third, the present studies do not provide unambiguous evidence that the principal biological contributions of CD38 upregulation to SSc pathogenesis are mediated via its outward-facing catalytic activity. The relative role of the ectoenzyme function of CD38 in disease pathogenesis can be addressed in future studies evaluating the impact of agents that selectively target CD38 ectoenzyme activity in disease models.

Resource availability

Lead contact

Further information and requests for resources should be directed to and will be fulfilled by the Lead Contact, John Varga (vargaj@umich.edu).

Materials availability

This study did not generate new unique reagents.

Data and code availability

This study did not generate data sets.

Methods

All methods can be found in the accompanying Transparent Methods supplemental file.

Author contributions

J.V., E.N.C., and B.S. generated the hypothesis, designed all experiments, analyzed the results, and prepared the manuscript. B.S., W.X.W., L.K., and S.B. conducted and performed *in vivo* and the main *in vitro* experiments. B.K., J.W., and J.G. analyzed gene expression in human and mouse samples. G.C.O., J.M.E.N., C.C.S.C., and E.N.C analyzed NAD metabolism. R.G.M., Q.W., D.G., and B.S. analyzed tissue morphology and expression levels and performed experiments with cultured cells. D.X., S.M., and M.A. performed flow cytometry and data analysis. P.C. determined lung fibrosis score. D.P. performed lung CT imaging and data analysis. All authors contributed to the preparation of the manuscript.

Declaration of interests

J.V. reports being a consultant for TeneoBio and Mitobridge. C.C.S.C. reports holding a patent on the use of CD38 inhibitors for metabolic diseases that is licensed by Elysium Health. E.N.C reports being a consultant for TeneoBio, Calico, Mitobridge, and Cyokinetics. E.N.C is on the advisory board of Eolo pharmaceutical, Argentina. J.G.'s research was support by grants from Lilly, Almirall, AbbVie, Kyowa Kirin, and BMS/Celgene; and he reports serving on the Advisory Board of Lilly, BMS, Novartis, Kyowa Kirin, AnaptysBio, and Almirall.

References

Akamata, K., Wei, J., Bhattacharyya, M., Cheresh, P., Bonner, M.Y., Arbiser, J.L., Raparia, K., Gupta, M.P., Kamp, D.W., and Varga, J. (2016). SIRT3 is attenuated in systemic sclerosis skin and lungs, and its pharmacologic activation mitigates organ fibrosis. Oncotarget 7, 69321–69336.

Aksoy, P., Escande, C., White, T.A., Thompson, M., Soares, S., Benech, J.C., and Chini, E.N. (2006a). Regulation of SIRT 1 mediated NAD dependent deacetylation: a novel role for the multifunctional enzyme CD38. Biochem. Biophys. Res. Commun. 349, 353–359.

Aksoy, P., White, T.A., Thompson, M., and Chini, E.N. (2006b). Regulation of intracellular levels of NAD: a novel role for CD38. Biochem. Biophys. Res. Commun. 345, 1386–1392.

Allanore, Y., Simms, R., Distler, O., Trojanowska, M., Pope, J., Denton, C.P., and Varga, J. (2015). Systemic sclerosis. Nat. Rev. Dis. Primers 1, 15002.

Asano, Y., and Varga, J. (2019). Rationally-based therapeutic disease modification in systemic sclerosis: novel strategies. Semin. Cell Dev. Biol. 101, 148–160.

Barbosa, M.T., Soares, S.M., Novak, C.M., Sinclair, D., Levine, J.A., Aksoy, P., and Chini, E.N. (2007). The enzyme CD38 (a NAD glycohydrolase, EC 3.2.2.5) is necessary for the development of diet-induced obesity. FASEB J. 21, 3629–3639.

Bhandari, R., Ball, M.S., Martyanov, V., Popovich, D., Schaafsma, E., Han, S., Eltanbouly, M., Orzechowski, N.M., Carns, M., Arroyo, E., et al. (2020). Profibrotic activation of human macrophages in systemic sclerosis. Arthritis Rheumatol. 72, 1160–1169.

Bhattacharyya, S., Tamaki, Z., Wang, W., Hinchcliff, M., Hoover, P., Getsios, S., White, E.S., and Varga, J. (2014). FibronectinEDA promotes chronic cutaneous fibrosis through Toll-like receptor signaling. Sci. Transl Med. 6, 232ra50.

Bhattacharyya, S., Wang, W., Morales-Nebreda, L., Feng, G., Wu, M., Zhou, X., Lafyatis, R., Lee, J., Hinchcliff, M., Feghali-Bostwick, C., et al. (2016).

Tenascin-C drives persistence of organ fibrosis. Nat. Commun. 7, 11703.

Bhattacharyya, S., Wang, W., Qin, W., Cheng, K., Coulup, S., Chavez, S., Jiang, S., Raparia, K., De Almeida, L.M.V., Stehlik, C., et al. (2018). TLR4-dependent fibroblast activation drives persistent organ fibrosis in skin and lung. JCI Insight 3, e98850.

Bhattacharyya, S., Wei, J., and Varga, J. (2011). Understanding fibrosis in systemic sclerosis: shifting paradigms, emerging opportunities. Nat. Rev. Rheumatol. 8, 42–54.

Bonkowski, M.S., and Sinclair, D.A. (2016). Slowing ageing by design: the rise of NAD(+) and sirtuin-activating compounds. Nat. Rev. Mol. Cell Biol. 17, 679–690.

Boslett, J., Helal, M., Chini, E., and Zweier, J.L. (2018a). Genetic deletion of CD38 confers post-ischemic myocardial protection through preserved pyridine nucleotides. J. Mol. Cell Cardiol. 118, 81–94.

Boslett, J., Hemann, C., Christofi, F.L., and Zweier, J.L. (2018b). Characterization of CD38 in the major cell types of the heart: endothelial cells highly express CD38 with activation by hypoxia-reoxygenation triggering NAD(P)H depletion. Am. J. Physiol. Cell Physiol. 314, C297–C309.

Boslett, J., Reddy, N., Alzarie, Y.A., and Zweier, J.L. (2019). Inhibition of CD38 with the Thiazoloquin(az)olin(on)e 78c Protects the Heart against Postischemic Injury. J. Pharmacol. Exp. Ther. 369, 55–64.

Braidy, N., Guillemin, G.J., Mansour, H., Chan-Ling, T., Poljak, A., and Grant, R. (2011). Age related changes in NAD+ metabolism oxidative stress and Sirt1 activity in wistar rats. PLoS One 6, e19194.

Camacho-Pereira, J., Tarrago, M.G., Chini, C.C., Nin, V., Escande, C., Warner, G.M., Puranik, A.S., Schoon, R.A., Reid, J.M., Galina, A., and Chini, E.N. (2016). CD38 dictates age-related NAD decline and mitochondrial dysfunction through an SIRT3-dependent mechanism. Cell Metab. 23, 1127–1139.

Canto, C., Menzies, K.J., and Auwerx, J. (2015). NAD(+) metabolism and the control of energy homeostasis: a balancing act between mitochondria and the nucleus. Cell Metab. 22, 31–53.

Chatterjee, S., Daenthanasanmak, A., Chakraborty, P., Wyatt, M.W., Dhar, P., Selvam, S.P., Fu, J.N., Zhang, J.Y., Nguyen, H., Kang, I.H., et al. (2018). CD38-NAD(+)axis regulates immunotherapeutic anti-tumor t cell response. Cell Metab. 27, 85.

Chini, C., Hogan, K.A., Warner, G.M., Tarrago, M.G., Peclat, T.R., Tchkonia, T., Kirkland, J.L., and Chini, E. (2019). The NADase CD38 is induced by factors secreted from senescent cells providing a potential link between senescence and age-related cellular NAD(+) decline. Biochem. Biophys. Res. Commun. 513, 486–493.

Chini, C.C.S., Peclat, T.R., Warner, G.M., Kashyap, S., Espindola-Netto, J.M., De Oliveira, G.C., Gomez, L.S., Hogan, K.A., Tarragó, M.G., Puranik, A.S., et al. (2020). CD38 ecto-enzyme in immune cells is induced during aging and regulates NAD+ and NMN levels. Nat. Metab. 2, 1284–1304.

Chini, C.C.S., Tarrago, M.G., and Chini, E.N. (2017). NAD and the aging process: role in life, death and everything in between. Mol. Cell Endocrinol. 455, 62–74.

Chiang, S.H., Harrington, W.W., Luo, G.Z., Milliken, N.O., Ulrich, J.C., Chen, J., Rajpal, D.K., Qian, Y., Carpenter, T., Murray, R., et al. (2015). Genetic ablation of CD38 protects against Western diet-induced exercise intolerance and metabolic inflexibility. PLoS One 10, e0134927.

Chini, E.N., Chini, C.C.S., Espindola Netto, J.M., De Oliveira, G.C., and Van Schooten, W. (2018). The pharmacology of CD38/NADase: an emerging target in cancer and diseases of aging. Trends Pharmacol. Sci. 39, 424–436.

Clement, J., Wong, M., Poljak, A., Sachdev, P., and Braidy, N. (2019). The plasma NAD(+) metabolome is dysregulated in "normal" aging. Rejuvenation Res. 22, 121–130.

Cockayne, D.A., Muchamuel, T., Grimaldi, J.C., Muller-Steffner, H., Randall, T.D., Lund, F.E., Murray, R., Schuber, F., and Howard, M.C. (1998). Mice deficient for the ecto-nicotinamide adenine dinucleotide glycohydrolase CD38 exhibit altered humoral immune responses. Blood 92, 1324–1333.

Costalonga, E.C., Fanelli, C., Garnica, M.R., and Noronha, I.L. (2020). Adipose-derived mesenchymal stem cells modulate fibrosis and inflammation in the peritoneal fibrosis model developed in uremic rats. Stem Cells Int. 2020, 3768718.

Da Silva, C.P., Schweitzer, K., Heyer, P., Malavasi, F., Mayr, G.W., and Guse, A.H. (1998). Ectocellular CD38-catalyzed synthesis and intracellular Ca2+-signalling activity of cyclic ADP-ribose in T-lymphocytes are not functionally related. FEBS Lett. 439, 291–296.

De Flora, A., Guida, L., Franco, L., and Zocchi, E. (1997). The CD38/cyclic ADP-ribose system: a topological paradox. Int. J. Biochem. Cell Biol. 29, 1149–1166.

Distler, J.H.W., Gyorfi, A.H., Ramanujam, M., Whitfield, M.L., Konigshoff, M., and Lafyatis, R. (2019). Shared and distinct mechanisms of fibrosis. Nat. Rev. Rheumatol. 15, 705–730.

Eckert, M.A., Coscia, F., Chryplewicz, A., Chang, J.W., Hernandez, K.M., Pan, S., Tienda, S.M., Nahotko, D.A., Li, G., Blazenovic, I., et al. (2019). Proteomics reveals NNMT as a master metabolic regulator of cancer-associated fibroblasts. Nature 569, 723–728.

Franks, J.M., Martyanov, V., Cai, G., Wang, Y., Li, Z., Wood, T.A., and Whitfield, M.L. (2019). a machine learning classifier for assigning individual patients with systemic sclerosis to intrinsic molecular subsets. Arthritis Rheumatol. 71, 1701–1710.

Frederick, D.W., Loro, E., Liu, L., Davila, A., Jr., Chellappa, K., Silverman, I.M., Quinn, W.J., 3rd, Gosai, S.J., Tichy, E.D., Davis, J.G., et al. (2016). Loss of NAD homeostasis leads to progressive and reversible degeneration of skeletal muscle. Cell Metab. 24, 269–282.

Ghosh, A.K., Bhattacharyya, S., Lafyatis, R., Farina, G., Yu, J.X., Thimmapaya, B., Wei, J., and Varga, J. (2013). p300 is elevated in systemic sclerosis and its expression is positively regulated by TGF-beta: epigenetic feed-forward amplification of fibrosis. J. Invest. Dermatol. 133, 1302–1310.

Ghosh, A.K., and Varga, J. (2007). The transcriptional coactivator and acetyltransferase p300 in fibroblast biology and fibrosis. J. Cell Physiol. 213, 663–671.

Gomes, A.P., Price, N.L., Ling, A.J., Moslehi, J.J., Montgomery, M.K., Rajman, L., White, J.P., Teodoro, J.S., Wrann, C.D., Hubbard, B.P., et al. (2013). Declining NAD(+) induces a pseudohypoxic state disrupting nuclear-mitochondrial communication during aging. Cell 155, 1624–1638.

Guarente, L. (2011). Franklin H. Epstein lecture: sirtuins, aging, and medicine. N. Engl. J. Med. 364, 2235–2244.

Hinz, B., and Lagares, D. (2020). Evasion of apoptosis by myofibroblasts: a hallmark of fibrotic diseases. Nat. Rev. Rheumatol. 16, 11–31.

Hinz, B., Phan, S.H., Thannickal, V.J., Prunotto, M., Desmouliere, A., Varga, J., De Wever, O., Mareel, M., and Gabbiani, G. (2012). Recent developments in myofibroblast biology: paradigms for connective tissue remodeling. Am. J. Pathol. 180, 1340–1355.

Ho, Y.Y., Lagares, D., Tager, A.M., and Kapoor, M. (2014). Fibrosis–a lethal component of systemic sclerosis. Nat. Rev. Rheumatol. 10, 390–402.

Hogan, K.A., Chini, C.C.S., and Chini, E.N. (2019). The multi-faceted ecto-enzyme CD38: roles in immunomodulation, cancer, aging, and metabolic diseases. Front Immunol. 10, 1187.

Johnson, S., and Imai, S.I. (2018). NAD (+) biosynthesis, aging, and disease. F1000Res 7, 132.

Kitamura, M., Nishino, T., Obata, Y., Oka, S., Abe, S., Muta, K., Ozono, Y., Koji, T., and Kohno, S. (2015). The kampo medicine Daikenchuto inhibits peritoneal fibrosis in mice. Biol. Pharm. Bull. 38, 193–200.

Liu, T., Rinke, A.E., Wang, J., and Phan, S.H. (2020). Cellular NAD+, fibroblast senescence and pulmonary fibrosis. FASEB J. 34, 1.

Malavasi, F., Deaglio, S., Funaro, A., Ferrero, E., Horenstein, A.L., Ortolan, E., Vaisitti, T., and Aydin, S. (2008). Evolution and function of the ADP ribosyl cyclase/CD38 gene family in physiology and pathology. Physiol. Rev. 88, 841–886.

Marangoni, R.G., Varga, J., and Tourtellotte, W.G. (2016). Animal models of scleroderma: recent progress. Curr. Opin. Rheumatol. 28, 561–570.

Massudi, H., Grant, R., Braidy, N., Guest, J., Farnsworth, B., and Guillemin, G.J. (2012). Age-associated changes in oxidative stress and NAD+ metabolism in human tissue. PLoS One 7, e42357.

Mori, Y., Ishida, W., Bhattacharyya, S., Li, Y., Platanias, L.C., and Varga, J. (2004). Selective inhibition of activin receptor-like kinase 5 signaling blocks profibrotic transforming growth factor beta responses in skin fibroblasts. Arthritis Rheum. 50, 4008–4021.

Peclat, T.R., Shi, B., Varga, J., and Chini, E.N. (2020). The NADase enzyme CD38: an emerging pharmacological target for systemic sclerosis, systemic lupus erythematosus and rheumatoid arthritis. Curr. Opin. Rheumatol. 32, 488–496.

Pham, T.X., Bae, M., Kim, M.B., Lee, Y., Hu, S., Kang, H., Park, Y.K., and Lee, J.Y. (2019). Nicotinamide riboside, an NAD+ precursor, attenuates the development of liver fibrosis in a diet-induced mouse model of liver fibrosis. Biochim. Biophys. Acta Mol. Basis Dis. 1865, 2451–2463.

Pissios, P. (2017). Nicotinamide N-methyltransferase: more than a vitamin B3 clearance enzyme. Trends Endocrinol. Metab. 28, 340–353.

Reinherz, E.L., Kung, P.C., Goldstein, G., and Schlossman, S.F. (1979). Separation of functional

subsets of human t-cells by a monoclonal antibody. Proc. Natl. Acad. Sci. U S A 76, 4061–4065.

Reyes, L.A., Boslett, J., Varadharaj, S., De Pascali, F., Hemann, C., Druhan, L.J., Ambrosio, G., El-Mahdy, M., and Zweier, J.L. (2015). Depletion of NADP(H) due to CD38 activation triggers endothelial dysfunction in the postischemic heart. Proc. Natl. Acad. Sci. U S A 112, 11648–11653.

Ryu, D., Zhang, H., Ropelle, E.R., Sorrentino, V., Mazala, D.A., Mouchiroud, L., Marshall, P.L., Campbell, M.D., Ali, A.S., Knowels, G.M., et al. (2016). NAD+ repletion improves muscle function in muscular dystrophy and counters global PARylation. Sci. Transl Med. 8, 361ra139.

Sargent, J.L., Li, Z., Aliprantis, A.O., Greenblatt, M., Lemaire, R., Wu, M.H., Wei, J., Taroni, J., Harris, A., Long, K.B., et al. (2016). Identification of optimal mouse models of systemic sclerosis by interspecies comparative genomics. Arthritis Rheumatol. 68, 2003–2015.

Shrimp, J.H., Hu, J., Dong, M., Wang, B.S., Macdonald, R., Jiang, H., Hao, Q., Yen, A., and Lin, H. (2014). Revealing CD38 cellular localization using a cell permeable, mechanism-based fluorescent small-molecule probe. J. Am. Chem. Soc. 136, 5656–5663.

Sosulski, M.L., Gongora, R., Feghali-Bostwick, C., Lasky, J.A., and Sanchez, C.G. (2017). Sirtuin 3 deregulation promotes pulmonary fibrosis. J. Gerontol. A. Biol. Sci. Med. Sci. 72, 595–602.

Sun, L., Adebanjo, O.A., Koval, A., Anandatheerthavarada, H.K., Iqbal, J., Wu, X.Y.,

Moonga, B.S., Wu, X.B., Biswas, G., Bevis, P.J., et al. (2002). A novel mechanism for coupling cellular intermediary metabolism to cytosolic Ca2+ signaling via CD38/ADP-ribosyl cyclase, a putative intracellular NAD+ sensor. FASEB J. 16, 302–314.

Tabib, T., Morse, C., Wang, T., Chen, W., and Lafyatis, R. (2018). SFRP2/DPP4 and FMO1/LSP1 define major fibroblast populations in human skin. J. Invest Dermatol. 138, 802–810.

Tarrago, M.G., Chini, C.C.S., Kanamori, K.S., Warner, G.M., Caride, A., De Oliveira, G.C., Rud, M., Samani, A., Hein, K.Z., Huang, R., et al. (2018). A potent and specific CD38 inhibitor ameliorates age-related metabolic dysfunction by reversing tissue NAD(+) decline. Cell Metab. 27, 1081–1095 e10.

Van Der Straaten, H.M., Canninga-Van Dijk, M.R., Verdonck, L.F., Castigliego, D., Borst, H.P., Aten, J., and Fijnheer, R. (2004). Extra-domain-A fibronectin: a new marker of fibrosis in cutaneous graft-versus-host disease. J. Invest Dermatol. 123, 1057–1062.

Varga, J., and Abraham, D. (2007). Systemic sclerosis: a prototypic multisystem fibrotic disorder. J. Clin. Invest. 117, 557–567.

Wei, J., Ghosh, A.K., Chu, H., Fang, F., Hinchcliff, M.E., Wang, J., Marangoni, R.G., and Varga, J. (2015). The histone deacetylase sirtuin 1 is reduced in systemic sclerosis and Abrogates fibrotic responses by targeting transforming growth factor beta signaling. Arthritis Rheumatol. 67, 1323–1334.

Yoshino, J., Baur, J.A., and Imai, S.I. (2018). NAD(+) Intermediates: the biology and therapeutic potential of NMN and NR. Cell Metab. 27, 513–528.

Yue, X., Yu, X., Petersen, F., and Riemekasten, G. (2018). Recent advances in mouse models for systemic sclerosis. Autoimmun. Rev. 17, 1225–1234.

Zerr, P., Palumbo-Zerr, K., Huang, J., Tomcik, M., Sumova, B., Distler, O., Schett, G., and Distler, J.H. (2016). Sirt1 regulates canonical TGF-beta signalling to control fibroblast activation and tissue fibrosis. Ann. Rheum. Dis. 75, 226–233.

Zhao, X., Kwan, J.Y.Y., Yip, K., Liu, P.P., and Liu, F.F. (2020). Targeting metabolic dysregulation for fibrosis therapy. Nat. Rev. Drug Discov. 19, 57–75.

Zhao, Y.J., Lam, C.M.C., and Lee, H.C. (2012). The membrane-bound enzyme CD38 exists in two opposing orientations. Sci. Signal. 5, ra67.

Zhou, C.C., Yang, X., Hua, X., Liu, J., Fan, M.B., Li, G.Q., Song, J., Xu, T.Y., Li, Z.Y., Guan, Y.F., et al. (2016). Hepatic NAD(+) deficiency as a therapeutic target for non-alcoholic fatty liver disease in ageing. Br. J. Pharmacol. 173, 2352–2368.

Zhu, X.H., Lu, M., Lee, B.Y., Ugurbil, K., and Chen, W. (2015). In vivo NAD assay reveals the intracellular NAD contents and redox state in healthy human brain and their age dependences. Proc. Natl. Acad. Sci. U S A 112, 2876–2881.

Supplemental Information

Targeting CD38-dependent NAD$^+$ metabolism

to mitigate multiple organ fibrosis

Bo Shi, Wenxia Wang, Benjamin Korman, Li Kai, Qianqian Wang, Jun Wei, Swarna Bale, Roberta Goncalves Marangoni, Swati Bhattacharyya, Stephen Miller, Dan Xu, Mahzad Akbarpour, Paul Cheresh, Daniele Proccissi, Demirkan Gursel, Jair Machado Espindola-Netto, Claudia C.S. Chini, Guilherme C. de Oliveira, Johann E. Gudjonsson, Eduardo N. Chini, and John Varga

Supplemental Information

Transparent Methods

Key Resources Table

REAGENT or RESOURCE	SOURCE	IDENTIFIER
Antibodies		
ASMA (h, m, r)*	Sigma-Aldrich	A2547
Collagen type I (h, m)	Southern Bio	1310-01
p-SMAD2/3 (h, m)	Cell Signaling	9520
CD38 (h)	Abcam	ab108403
CD38 (m)	R&D	HAF016
NNMT (h, m)	Abcam	ab119758
β-actin (h, m, r)	Sigma	A5316
Ac-Lysine	Cell Signaling	9520
P300 (h, m, r)	Santa Cruz	48343
F4/80 (m)	Cell Signaling	70076T
CD68 (h, m, r)	Abcam	Ab125212
Fibronectin-EDA	Sigma	SAB4200784

*h, human; r, rat; m, mouse

REAGENT or RESOURCE	SOURCE	IDENTIFIER
CHEMICALS, PEPTIDES, AND RECOMBINANT PROTEIN		
CD78 inhibitor (78c)	GlaxoSmithKline	GSK3010460B
Nicotinamide Riboside	ChromaDex	ASB-00014332
Recombinant human CD38	R&D system	2404-AC
Chlorhexidine gluconate	Sigma	C9394
Recombinant human TGF-β2	PeproTech	100-35B
Recombinant human TNF-α	PeproTech	300-01A
Recombinant human IL13	PeproTeck	200-13

REAGENT or RESOURCE	SOURCE	IDENTIFIER
CRITICAL COMMERCIAL ASSAYS		
NAD/NADH Quantitation Kit	Sigma-Aldrich	MAK037
NAD/NADH-Glo Assay	Promega	G9071
Hydroxyproline Assay Kit	Bio Vision	K555-100
Quick-RNA MiniPrep Kit	Zymo Research	Cat# 11-328
RNeasy Fibrous Tissue Mini Kit	QIAGEN	74704
U-PLEX biomarker Group 1 assays, SECTOR	Meso Specific Discovery	K15069L-1

REAGENT or RESOURCE	SOURCE	IDENTIFIER
EXPERIMENTAL ANIMALS		
CD38 KO mice	The Jackson Laboratory	B6.129P2-*Cd38tm1Lnd*/J
C57BL6 wild-type mice	The Jackson Laboratory	
Aged mice (12, 18 month)	National Institute on Aging	

REAGENT or RESOURCE	SOURCE	IDENTIFIER
PCR PRIMERS AND REAGENTS		
mCol1A1 RT-qPCR forward 5'-AGCCGCAAAGAGTCTACATG-3'	Integrated DNA Technologies	
mCol1A1 RT-qPCR reverse: 5'-CTTAGGCCATTGTGTATGCAG-3'	Integrated DNA Technologies	
mASMA RT-qPCR forward 5'-ATGCAGAAGGAGATCACAGC-3'	Integrated DNA Technologies	
mASMA RT-qPCR reverse 5'-GTATTCCTGTTTGCTGATCCAC-3'	Integrated DNA Technologies	
mGAPDH RT-qPCR forward 5'-ATCTTCTTGTGCAGTGCCAGC-3'	Integrated DNA Technologies	
mGAPDH RT-qPCR reverse 5'-GTTGATGGCAACAATCTCCAC-3'	Integrated DNA Technologies	
hFn-EDA RT-qPCR forward 5'TAAAGGACTGGCATTCACTGA3'	Integrated DNA Technologies	
hFn-EDA RT-qPCR reverse 5' GTGCAAGGCAACCACACTGAC3'	Integrated DNA Technologies	
hCol1A1 RT-qPCR forward 5'-TGGTGTGCAAGGTCCC-3'	Integrated DNA Technologies	
hCol1A1 RT-qPCR reverse 5'-CATTCCCTGAAGGCCAG-3'	Integrated DNA Technologies	

hASMA RT-qPCR forward 5'-CAGGGCTGTTTTCCCATCCAT-3'	Integrated DNA Technologies	
hASMA RT-qPCR reverse 5'-GCCATGTTCTATCGGGTACTTC-3'	Integrated DNA Technologies	
hGAPDH RT-qPCR forward 5'-CATGAGAAGTATGACAACAGCCT-3'	Integrated DNA Technologies	
hGAPDH RT-qPCR reverse 5'-AGTCCTTCCACGATACCAAAGT-3'	Integrated DNA Technologies	

ANTI-MOUSE ANTIBODIES USED FOR FLOW CYTOMETRY		
REAGENTS	SOURCE	IDENTIFIER (clone)
CD45 V500	BD Biosciences	30-F11
Siglec F Alexa 647	BD Biosciences	E50-2440
CD11c APC-Cy7	BioLegend	N418
Ly6C PE	BioLegend	HK1.4
CD80 BV605	BioLegend	16-10A1
CD86 BV605	BioLegend	GL-1
CD11b BV421	BioLegend	M1/70
Cd64 PE-Cy7	BioLegend	X54-5/7
Ly6G PerCP5.5	BioLegend	1A8
I-A/I-E FITC	BioLegend	M5/114.15.2
CD3 Alexa 700	BioLegend	500A2
CD44 APC-Cy7	BioLegend	IM7
TCR$\gamma\delta$ APC	BioLegend	GL3
CD45 V500	BioLegend	30-F11
CD69 BV605	BioLegend	H1.2F3
CD62L PE-Cy7	BioLegend	MEL-14
CD25 PE	BioLegend	3C7
CD11b V500	BioLegend	M1/70
CD38 PE-Cy7	BioLegend	90

MARCO APC	BioLegend	FAB2956A
CD8 Alexa700	BioLegend	53-6.7
FoxP3 Per CP-Cy5.5	BioLegend	FJK-16s
iNOS PE-Cy7	eBioscience	25-5920-80
EgR2 PE	eBioscience	12-6691-82
CD206 APC	eBioscience	141708

Method Details

Mouse fibrosis models

Bleomycin model: Animal protocols were institutionally approved by the Animal Care and Use Committees of Northwestern University. We used 18 months-old C57BL/6J female wild-type (National Institute on Aging, NIA) and 12 months-old CD38KO mice on the C57BL/6 background (B6.129P2-*CD38^{tm1Lnd}*/J, Jackson laboratory) as previously described (Camacho-Pereira et al., 2016, Cockayne et al., 1998, Guedes et al., 2006). For *in vivo* experiments, mice were randomized to receive vehicle, bleomycin, or bleomycin in combination with CD38 inhibitor 78c (GlaxoSmithKline, Philadelphia, PA) (Haffner et al., 2015). Mice were fed a standard chow diet or chow supplemented with nicotinamide riboside (NR, 3g/kg chow) (ChromaDex, Irvine, CA). 78c was dissolved in 0.5% (w/v), K-15 HPMC (Sigma H7509), and 0.1% (w/v) Tween 80 and administered by daily gavage feeding (30 mg/kg) (Tarrago et al., 2018, Haffner et al., 2015). Mice were given daily subcutaneous (s.c.) injections of PBS or bleomycin (10 mg/kg, Teva Pharmaceuticals, North Wales, PA) in parallel for 14 d. Mice were sacrificed on day 21, and lesional skin and lungs were harvested. Tissue collagen content was determined by hydroxyproline assays (Bhattacharyya et al., 2018a).

Peritoneal membrane fibrosis: Wild-type (from NIA) and CD38 null C57BL/6J male mice were used. Peritoneal membrane fibrosis was induced by alternate-daily i.p. injections (0.3ml, 10 injections) of 0.1% chlorhexidine gluconate (CG, Sigma, C9394) dissolved in 15% ethanol/PBS, while mice in the control group received i.p. injections of 15% ethanol/PBS solvent only. Mice were maintained on a diet of chow supplemented with NR (3 g/kg chow), and daily oral gavage with 78c (30 mg/kg). At day 19, mice were sacrificed, and peritoneal tissues were carefully

dissected, and peritoneal membrane thickness (submesothelial compact zone superficial to the abdominal wall muscles) was determined (Bhattacharyya et al., 2018a, Yokoi et al., 2012) .

Cell cultures

Primary cultures of human dermal fibroblasts were established by explantation from neonatal foreskin or from adult forearm skin biopsies of SSc patients or matched healthy control subjects (Bhattacharyya et al., 2016). Primary dermal fibroblasts were also established from wild-type and CD38-null mice. Early–passage (<5) fibroblasts were grown in monolayers in 6-well plastic dishes or 100 mm plates (Corning Incorporated) and studied at early confluence (Bhattacharyya et al., 2013). Cultures of mouse and human fibroblasts were maintained in DMEM supplemented with 10% FBS (Thermo Fisher Scientific), 1% vitamin solutions, 2 mM L-glutamine, and 120 Units/ml penicillin and streptomycin (Lonza, Alpharetta, GA). To test fibrotic response, confluent fibroblasts were incubated in serum-free media containing 10 ng/ml TGF-β2 (Peprotech, Rocky Hill, NJ, 100-21) and 0.1% BSA (Sigma, St. Louis, MO). Indicated reagents were added 2 h prior to TGF-β2 (Chavez et al., 2011). To induce CD38 in fibroblasts, human skin fibroblasts at exponential growth in complete DMEM culture medium were co-incubated with TNF-α (10ng/ml), TGF-β2 (10ng/ml) or IL-13(10ng/ml) for 24 hours.

To generate bone marrow-derived macrophage (BMDM), femurs and tibias from wild type and CD38-null mice were harvested and cultured as previously described (Jablonski et al., 2016). Briefly, isolated cells were incubated in Dulbecco's Modified Eagle Media (DMEM, Mediatech, Herndon, VA) supplemented with 10% heat-activated fetal bovine serum (FBS) (Life Technologies, Grand Island, NY), 1% penicillin/streptomycin, 1% glutamine, and 20% L929 cell

culture supernatant which contains macrophage colony stimulating factor. On day 8, cells were

re-seeded into 24-well plates, and incubated with media alone (unstimulated M0 condition) or

M1-activated with LPS (100 ng/ml, Sigma-Aldrich L2880) + mIFN-γ (20ng/mL, R&D 485-MI/CF)

or alternatively/M2-activated with IL-4 (20 ng/mL, R&D 404-ML/CF) + mIL-13 (20 ng/ml, R&D

413-ML/CF) for 24 hours. CD38i (78c, 0.5μM) and NR (100 μM) were added after reseeding, and

cells were harvested at the indicated time-points for RNA and protein isolation or flow

cytometric analysis.

RNA isolation and qPCR analysis

Total RNA from cultured human and mouse fibroblasts, macrophages or mouse tissues was

isolated by Quick RNA miniprep kit (Zimo Research, Irvine, CA, 11-328) or /by RNeasy Fibrous

tissue mini kits (Qiagen, Germantown, MD, 74704). Reverse transcription of RNA to cDNA was

performed using Supermix (cDNA Synthesis Supermix; Quanta Biosciences, Beverly, MA) as

described (Bhattacharyya et al., 2016). Amplification products (50 ng) were amplified using SYBR

Green PCR Master Mix or TagMan gene expression assay (Applied Biositems, Foster city, CA) on

an Applied Biosystems 7500 Prism Sequence Detection System. Gene expression was normalized

to internal GAPDH, and -fold change was calculated (Bhattacharyya et al., 2018b). Primer

sequences are shown in Key Resources Table.

Immunoblotting

At the end of the experiments, cells or mouse tissues were harvested, whole cell lysates

prepared, and equal amounts of proteins subjected to Western blot analysis as described

([Bhattacharyya et al., 2013](#)). Primary and secondary antibodies used are listed in Key Resources Table (Antibodies). Band intensities in Western blot were photo scanned and quantitated using ImageJ (NIH) and normalized to β-actin or GAPDH.

Transient transfection and luciferase assays

Subconfluent foreskin fibroblasts were transiently transfected with $(SBE)_4$-luc plasmids using SuperFect transfection reagent (Qiagen, Germantown, MD). Following 24 h incubation, cultures were harvested and whole cell lysates were assayed for their luciferase activities ([Bhattacharyya et al., 2016](#)). All experiments were performed in triplicates.

Immunofluorescence confocal microscopy

Foreskin fibroblasts were seeded on glass coverslips and studied by immunofluorescence as described ([Bhattacharyya et al., 2018a](#), [Fang et al., 2016](#)). The antibodies used are described in Key Resource Table (Antibodies). Fibroblasts at 80% confluence were fixed in 3.7% paraformaldehyde, permeabilized, and incubated with antibodies to α-SMA (MilliporeSigma, St. Louis, MO) or phospho-Smad2 (Cell Signaling Technology Inc., Danvers, MA, 3018) at 1:100 dilution, followed by Alexa Fluor–labeled secondary antibodies (Invitrogen, Norcross, GA). Nuclei were counterstained with DAPI. Subcellular distribution of immunofluorescence was evaluated under an immunofluorescence microscope or Zeiss UV Meta 510 confocal microscope or a Nikon C2 or A1Si confocal microscope and quantitated using Image J.

Determination of NAD⁺ consumer/biosynthesis enzyme expression in SSc skin biopsies and in murine models

To determine levels of NAD⁺ consumer and biosynthesis enzymes in SSc, we queried publicly available multiple genome-wide skin biopsy-based transcriptome datasets. First, we queried (GSE76886 https://www.ncbi.nlm.nih.gov/geo/query/acc.cgi?acc=GSE76886), comprised of baseline skin biopsies from 68 SSc patients (12 limited and 56 diffuse cutaneous disease) and 22 healthy controls. Two additional datasets (PRESS and SPARC) from independent patient cohorts were used to validate the results. GSE130955 (PRESS) cohort (https://www.ncbi.nlm.nih.gov/geo/query/acc.cgi?acc=GSE130955) analyzed global gene expression from skin biopsies of 48 patients with early diffuse cutaneous SSc and 33 matched healthy controls (Skaug et al., 2020). The SPARC cohort used RNA-seq generate genome wide transcriptome profiles from 14 healthy control and 20 SSc (6 lcSSc and 14 dcSSc) skin biopsies (Roberson et al., 2016). Transcript levels in each biopsy were centered on their median values across all arrays.

To correlate gene expression levels to modified Rodnan skin score (MRSS) in each biopsy, profibrotic signaling pathways were analyzed using Pearson's correlation coefficient test. Pathway gene signatures of TGF-β and PDGF were defined as all genes ≥ 2-fold up- or down-regulated across all of their corresponding 12 and 24 hour time points in cultured human dermal fibroblasts relative to untreated controls (Johnson et al., 2015). SIRT1 signature genes were extracted from published datasets (Beane et al., 2012). SIRT1 pathway scores, defined as Pearson's correlation coefficients of each pathways, were used to quantify the contribution of a specific pathway to the gene expression within a given patient. (Johnson et al., 2015). Mann

Whitney *U* test and 1-way ANOVA method were used to analyze differences between groups.

Additionally, we queried skin gene expression data from mice with experimentally-induced

scleroderma (GSE71999 (Sargent et al., 2016), and GSE13289)

(https://www.ncbi.nlm.nih.gov/geo/query/acc.cgi?acc=GSE132869).

Histology and Immunohistochemistry

4-µm thick sections of formalin-fixed, paraffin-embedded skin biopsy samples from SSc patients,

healthy subjects or from mouse skin tissue and lungs were analyzed by immunohistochemistry,

as described (Bhattacharyya et al., 2018a). Demographic and clinical features of Healthy subject

and SSc patient skin biopsies used for CD38 expression were listed in Table 1. Slides were

incubated with anti-mouse CD38 (Abcam, Cambridge, MA, ab230153), anti-mouse or human

SMA (Sigma, St. Louis, MO, A2547), F4/80 (Cell Signaling, 70076T) and mouse CD68 (Abcam,

ab125212), human CD38 (Abcam, ab108403) antibodies, or isotype-matched control IgG

(eBioscience, San Diego, CA) followed by HRP-conjugated secondary antibody which was

visualized with diaminobenzidine substrate, and counterstained with hematoxylin.

Immunopositive cells were counted in 5 randomly selected high-power fields (hpf, 40X

objective) per biopsy specimen by an observer in a blinded manner (Fang et al., 2016). One-way

ANOVA was used for statistic significant analysis.

Supplemental Table 1. Demographic and clinical features of subjects (skin biopsies used for IHC analysis, related to Figure 1H and 1I).

Identifier	Age (years)	Sex	Race	Diagnosis	Disease duration (months)	MRS[*]
SPARC_SSc_02	31	Female	Hispanic	dcSSc	40	6
SPARC_SSc_19	36	Female	Hispanic	dcSSc	24	17
SPARC_SSc_15	30	Male	White	lcSSc	28	17
SPARC_SSc_16	45	Female	Black	dcSSc	56	11
SPARC_SSc_05	60	Male	White	lcSSc	44	6
SPARC_SSc_31	60	Female	White	dcSSc	12	36
SPARC_SSc_06	69	Male	White	dcSSc	12	41
SPARC_SSc_07	50	Female	White	dcSSc	9	24
SPARC_SSc_10	40	Female	White	dcSSc	72	16
SPARC_SSc_11	64	Female	White	dcSSc	8	33
SPARC_NORM_08	28	Female	Hispanic	Control	N/A	N/A
RegNorm_1015	35	Female	Hispanic	Control	N/A	N/A
SPARC_NORM_05	26	Male	White	Control	N/A	N/A
RegNorm_1026	56	Male	White	Control	N/A	N/A

*dcSSc, diffuse cutaneous SSc; MRSS, modified Rodnan skin score (0-51)

Measurement of skin and lung fibrosis

Dermal thickness was determined at 5 randomly selected sites as previously described (Bhattacharyya et al., 2016). Ashcroft score, reflecting both severity and extent of lung fibrosis (Ashcroft et al., 1988) was determined in a blinded manner by a pulmonary pathologist.

Measurement of NAD metabolism

Levels of NAD^+ in confluent human fibroblast cultures and mouse skin, lung and liver were measured using NAD/NADH quantification kits according to manufacturer's instructions (Sigma-Aldrich, MAK037). NAD^+ levels in serum were measured using NAD/NADH Glo Assay kit (Promega, G9071) Tissue levels of NAD^+ and its metabolites were also determined by Ultra-performance

Liquid Chromatography (UPLC)-Mass Spectrometry ([de Oliveira et al., 2018](#), [Kanamori et al., 2018](#)). In brief, harvested tissues were immediately immersed in 10% TCA (Sigma, St. Louis, MO, T6399), snap frozen in liquid nitrogen, and preserved at -80°C. Samples were then thawed on ice and levels of NAD$^+$, nicotinamide mononucleotide (NMN), and nicotinamide riboside (NR) were determined using cycling assay employing UPLC-Mass spectrometry ([Camacho-Pereira et al., 2016](#)).

Microcomputed lung tomography

Lung computed tomography (CT) images were acquired using a Mediso NANOSCAN8 PETCT system (Mediso USA) using 50KeV energy, an exposure time of 300 msec for each projection for a total of 710 projections per mouse. 3D images were reconstructed with a final isotropic spatial resolution of 100 micrometers. Mice were maintained under anesthesia delivered through a nose cone with isofluorane mixed with 100% oxygen in a supine position. 3-D images were exported off-line in DICOM format and analyzed using threshold segmentation algorithms provided in ITK-SNAP software ([Yushkevich et al., 2006](#)). Varying Hounsfeld units (HU) threshold windows were used to differentiate healthy tissue from fibrotic lung tissue. Total lung volume for each mouse was determined using a threshold window that enabled masking of whole lung and removal of surrounding tissue (HU 1000-500). Two thresholds were then used to acquire "normal tissue" (-1000 - -100 HU) and "abnormal/fibrotic tissue" (-100 - +500 Hu). The three sets of volumetric data corresponding to different threshold windows were generated for each of the mice scanned for each cohort. The control group (i.e. no fibrosis) was used as a standard reference value to generate the index factors (lung fibrotic index).

Flow cytometry

Flow cytometry analysis of the skin, lungs and spleen was performed as described ([Misharin et al., 2013](#), [Prasad et al., 2018](#), [Bharat et al., 2016](#)). Briefly, at sacrifice organs were harvested, perfused with PBS and cut into small pieces and processed in digestion buffer (1 mg/ml of Collagenase D and 0.1 mg/ml DNase I, both from Roche, Indianapolis, IN), using GentleMACS dissociator (Miltenyi). Homogenized tissues were passed through 40-μm nylon mesh to obtain a single-cell suspension. The red blood cells were lysed using BD Pharm Lyse (BD Biosciences, Cat# 555899). Cells were incubated with mouse Fc-block (Cat# 553142, BD Biosciences, San Jose, CA) followed by appropriate antibody cocktails. These antibodies included CD45, CD11b, CD11c, Ly6C, Ly6G, MHC II, CD80, CD86, B220, CD3, CD4, CD8, and CD38 (all from BioLegend, San Diego, CA, and eBioscience). Live/dead fixable blue (Cat# L-23105, Invitrogen, Carlsbad, CA) was added to the cells thereafter to label dead cells prior to cell fixation with 0.5% formaldehyde diluted with PBS. Each incubation step was performed at 4°C for 30 minutes in dark. Antibodies are listed in Key Resources with the antigen, conjugated fluorophore, and clone specified. A 6-laser Fortessa flow cytometer (BD Biosciences) was used to enumerate cell populations and the data was analyzed using FlowJo software (TreeStar, Ashland, OR). For *ex vivo* differentiation assays, bone marrow-derived macrophages were fixed and permeabilized using thexP3 staining buffer kit s(eBioscience), and immunostained with antibodies to inducible nitric oxide synthase (iNOS), EgR2, and CD206 (Key Resources Table). Cells were acquired on a BD Fortessa and analyzed using BD FlowJo version 9. As controls, fluorescence minus one (FMO) was used to place the gates for analysis.

Statistics

Data are presented as means ± SEM. Two-tailed Student's t test or Mann Whitney U test was used for comparisons between 2 groups. If experiment involved more than three groups, 1-way ANOVA followed by Tukey analysis was used to examine for statistical significance. The Chi Square analysis was used for categorical variables. A p value less than 0.05 denoted the presence of statistically significant difference. The Pearson correlation for continuous variables and the Spearman correlation for ordinal variables were used to evaluate relationships between two variables. Data were analyzed and graphs were created using GraphPad prism (GraphPad Prism Software version 7.03, GraphPad Software Inc.).

Study approvals

All animal studies were conducted in accordance with NIH guidelines for the care and use of laboratory animals and protocols were approved by the IACUC of Northwestern University. Studies involving human subjects were approved by the IRB of Northwestern University, and all participants provided written informed consent.
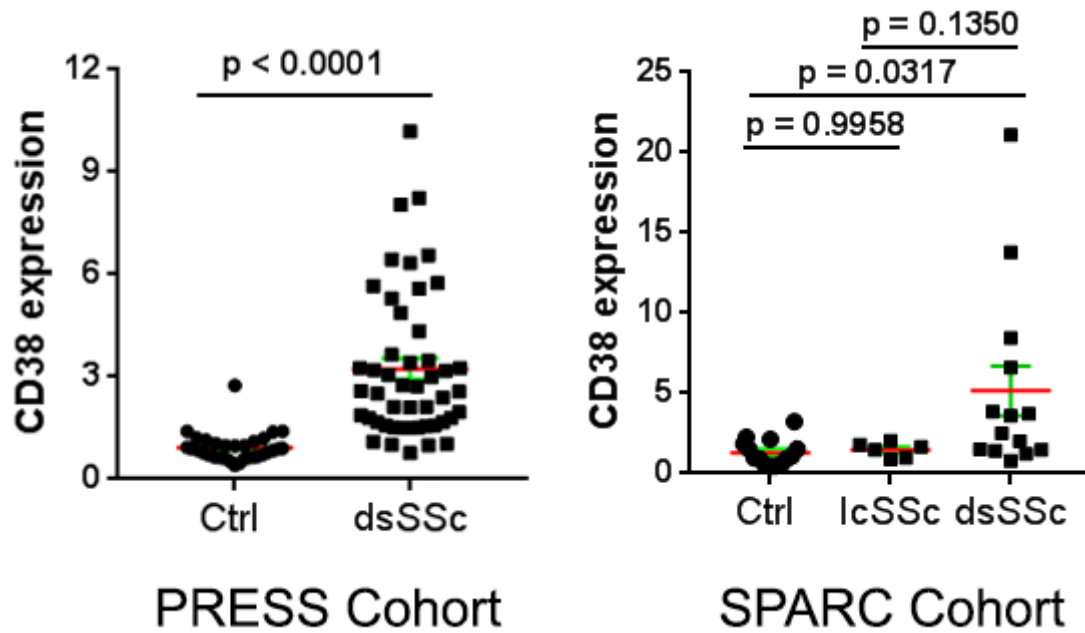
Figure S1 (related to Figure 1). Significantly elevated CD38 mRNA in SSc skin biopsies in two independent patient cohorts. The PRESS cohort dataset (GSE130955) comprises global gene expression data from skin biopsies of 48 patients with early diffuse cutaneous SSc and 33 matched healthy controls. The SPARC cohort comprises global gene expression data (RNA-seq) from skin biopsies of 20 patients with SSc (6 lcSSc and 14 dcSSc) and 14 healthy controls. Error bars, means ± SEM.
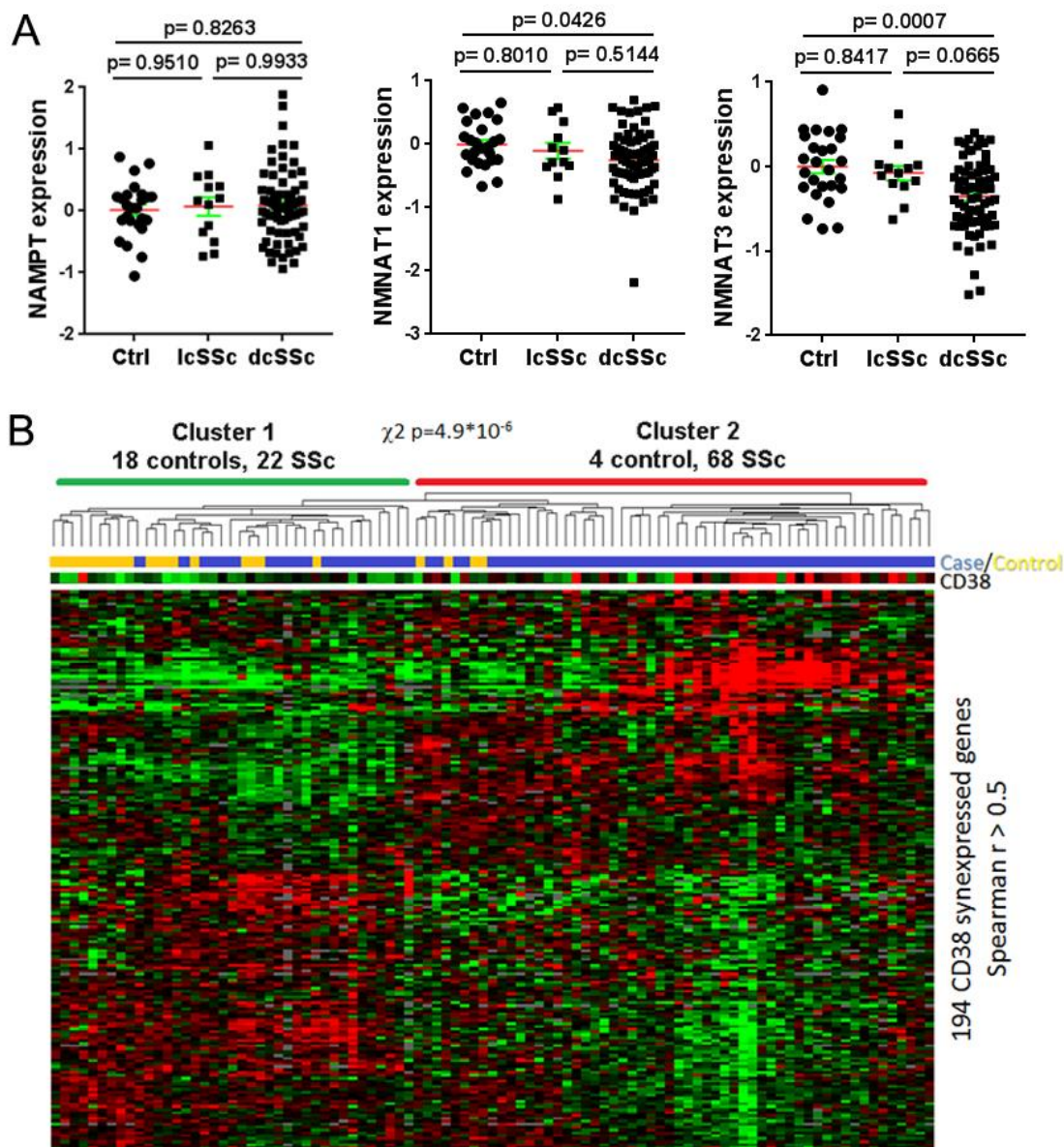
Figure S2 (related to Figure 1). Interrogating skin biopsy transcriptomes: healthy control and SSc skin biopsies. Gene expression from SSc and control individuals' skin was assessed (GEO accession GSE76886). (A) Expression of NAD$^+$ salvage pathway enzymes NAMPT, NMNAT1, and NMNAT3 in healthy controls, lcSSc and dcSSc biopsies. Error bars are means ± SEM. (B) A 194-gene CD38 co-expression gene module (genes with Spearman correlation r>0.5 with CD38) is able to discriminate SSc from healthy control skin biopsies using hierarchical clustering.
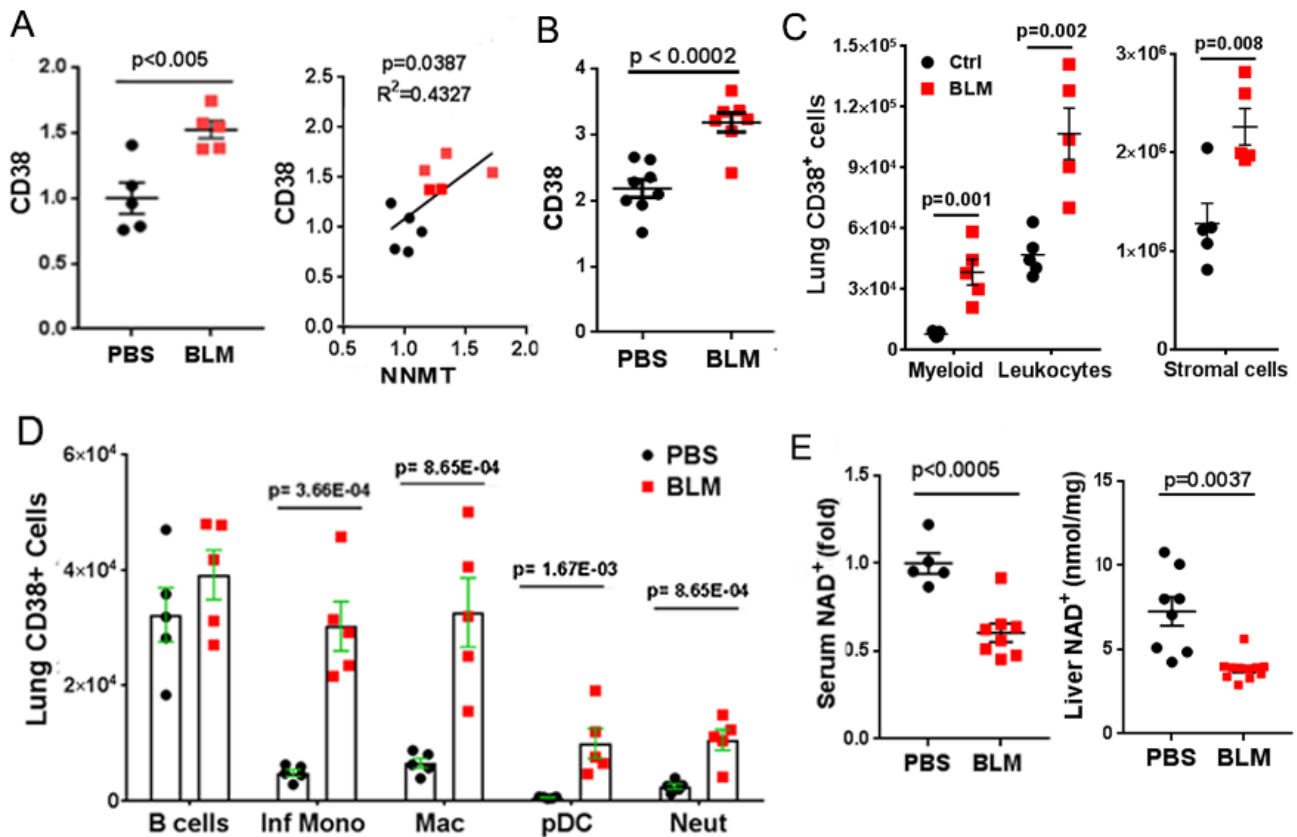
Figure S3. Elevated CD38 associated with reduced NAD$^+$, related to Figure 1. (A) Elevated CD38 mRNA levels in skin from bleomycin-treated mice (d 21). Analysis of dataset GSE71999. Right panel, CD38 levels correlated with NNMT levels in same skin biopsies. (B) Elevated CD38 mRNA in an independent mouse experiment (GSE13289). (C), (D) Flow cytometry of lung cells from bleomycin-treated and control mice. Elevated numbers of CD38+ hematopoietic (left panel) and stromal (right panel) cell populations. (D) CD38-positive inflammatory cell subpopulations. (E) Levels of circulating and tissue (liver) NAD$^+$ in bleomycin-treated mice (NAD$^+$ measured as described under Methods). Bar graphs are means ± SEM.
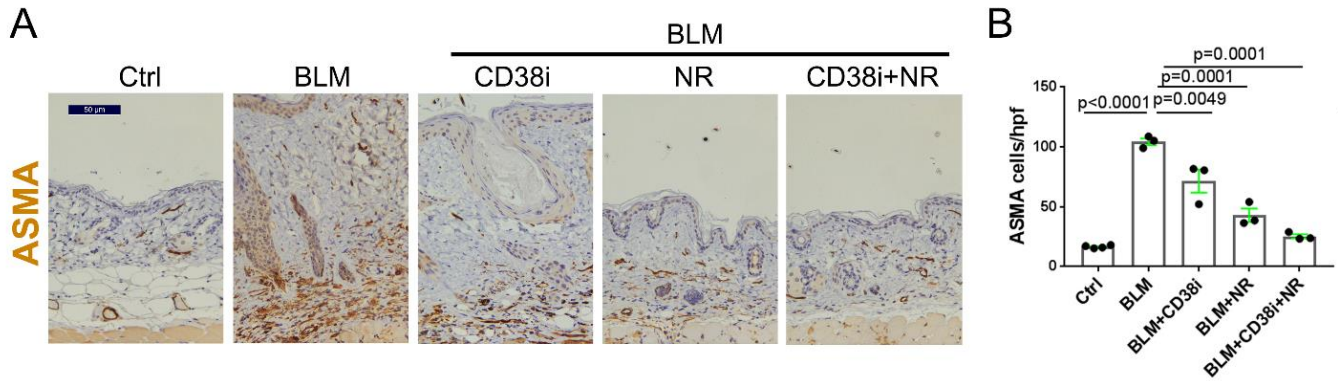
Figure S4 (related to Figure 3). **CD38 inhibitor and NR supplementation reduced skin myofibroblast accumulation in bleomycin-treated mice.** (A) Immunohistochemistry of skin from mice treated with NR supplementation and 78c (CD38i) alone or in combination using antibodies against alpha smooth muscle actin (ASMA); representative images. Scale bar length: 50 μm. (B) Quantification of myofibroblasts within the lesional dermis. ASMA-positive interstitial cells were counted in 5 randomly selected high-power fields (hpf, 40 x objective, scale bar = 50 μm) per slide. Bars are means ± SEM (one-way ANOVA).
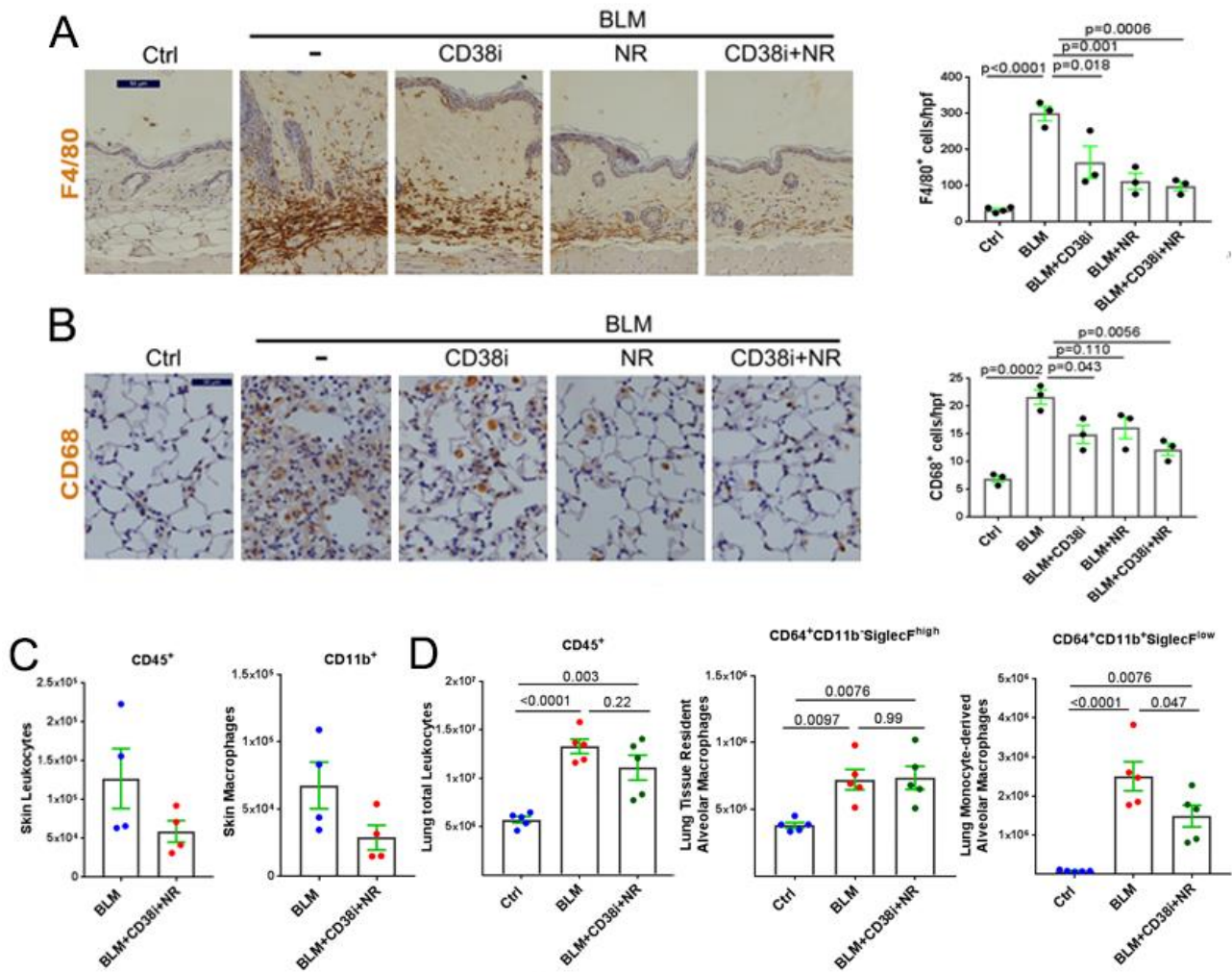
Figure S5 (related to Figure 3). CD38 inhibitor 78c and NR attenuated bleomycin-induced skin and lung inflammation. C57/BL6 mice were treated with s.c. bleomycin and CD38 inhibitor (30 mg/kg by gavage) plus NR supplementation (3g/kg chow). Mice were sacrificed at day 21 and skin and lungs harvested for analysis. (A and B) Immunohistochemistry of skin (A) and lung (B) using antibodies to F4/80 or CD68. Representative images (left panels); scale bar length: 50 μm. quantification of immunopositive cells (right panels). (C and D) Flow cytometry analysis of inflammatory cells in skin and lungs. Immunopositive cells were counted in 5 randomly selected high-power fields (hpf, 40 x objective) per slide. Bars are means ± SEM.
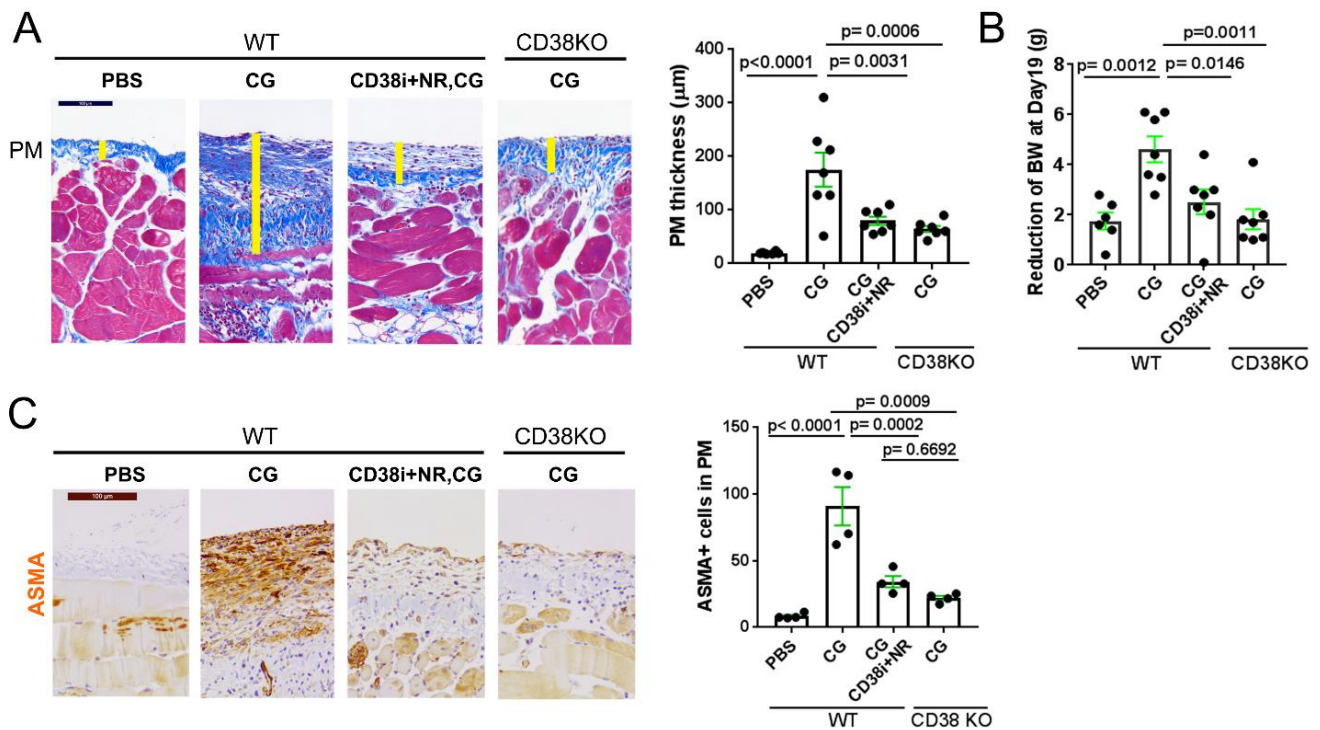
Figure S6 (related to Figure 3). Genetic or pharmacological targeting of CD38 ameliorates peritoneal fibrosis. 15 month-old wild-type and CD38 null C57BL/6J male mice were used. Peritoneal membrane fibrosis was induced by alternate-daily i.p. injections 0.1% chlorhexidine gluconate for 19 days. Mice were maintained on standard chow or NR-supplemented chow diet (3g/kg) plus daily oral gavage with 78c (30 mg/kg BW). Mice were sacrificed at day 19, and parietal peritoneal membranes were harvested for analysis. (A) Left panel, Masson's trichrome stain, and representative images. Right panel, submesothelial compact zone thickness was indicated by yellow bar. (B) Weight loss of mice groups. (C) Immunostaining with antibodies to ASMA. Representative images (left). Scale bar length in (A and C): 100 μm. Quantitation of F4/80-positive cells in the peritoneal membrane (right panel). All bar graphs are means ± SEM. One-way ANOVA followed by Tukey post hoc tests was used for statistic significant analysis.

Supplemental References

Ashcroft, T., Simpson, J. M. & Timbrell, V. 1988. Simple method of estimating severity of pulmonary fibrosis on a numerical scale. *J Clin Pathol,* 41**,** 467-70.

Beane, J., Cheng, L., Soldi, R., Zhang, X., Liu, G., Anderlind, C., Lenburg, M. E., Spira, A. & Bild, A. H. 2012. SIRT1 pathway dysregulation in the smoke-exposed airway epithelium and lung tumor tissue. *Cancer Res,* 72**,** 5702-11.

Bharat, A., Bhorade, S. M., Morales-Nebreda, L., Mcquattie-Pimentel, A. C., Soberanes, S., Ridge, K., Decamp, M. M., Mestan, K. K., Perlman, H., Budinger, G. R. & Misharin, A. V. 2016. Flow Cytometry Reveals Similarities Between Lung Macrophages in Humans and Mice. *Am J Respir Cell Mol Biol,* 54**,** 147-9.

Bhattacharyya, S., Kelley, K., Melichian, D. S., Tamaki, Z., Fang, F., Su, Y., Feng, G., Pope, R. M., Budinger, G. R., Mutlu, G. M., Lafyatis, R., Radstake, T., Feghali-Bostwick, C. & Varga, J. 2013. Toll-like receptor 4 signaling augments transforming growth factor-beta responses: a novel mechanism for maintaining and amplifying fibrosis in scleroderma. *Am J Pathol,* 182**,** 192-205.

Bhattacharyya, S., Wang, W., Morales-Nebreda, L., Feng, G., Wu, M., Zhou, X., Lafyatis, R., Lee, J., Hinchcliff, M., Feghali-Bostwick, C., Lakota, K., Budinger, G. R., Raparia, K., Tamaki, Z. & Varga, J. 2016. Tenascin-C drives persistence of organ fibrosis. *Nat Commun,* 7**,** 11703.

Bhattacharyya, S., Wang, W., Qin, W., Cheng, K., Coulup, S., Chavez, S., Jiang, S., Raparia, K., De Almeida, L. M. V., Stehlik, C., Tamaki, Z., Yin, H. & Varga, J. 2018a. TLR4-dependent fibroblast activation drives persistent organ fibrosis in skin and lung. *JCI Insight,* 3**,** e98850.

Bhattacharyya, S., Wang, W., Tamaki, Z., Shi, B., Yeldandi, A., Tsukimi, Y., Yamasaki, M. & Varga, J. 2018b. Pharmacological Inhibition of Toll-Like Receptor-4 Signaling by TAK242 Prevents and Induces Regression of Experimental Organ Fibrosis. *Front Immunol,* 9**,** 2434.

Camacho-Pereira, J., Tarrago, M. G., Chini, C. C., Nin, V., Escande, C., Warner, G. M., Puranik, A. S., Schoon, R. A., Reid, J. M., Galina, A. & Chini, E. N. 2016. CD38 Dictates Age-Related NAD Decline and Mitochondrial Dysfunction through an SIRT3-Dependent Mechanism. *Cell Metab,* 23**,** 1127-39.

Chavez, S. A., Martinko, A. J., Lau, C., Pham, M. N., Cheng, K., Bevan, D. E., Mollnes, T. E. & Yin, H. 2011. Development of beta-amino alcohol derivatives that inhibit Toll-like receptor 4 mediated inflammatory response as potential antiseptics. *J Med Chem,* 54**,** 4659-69.

Cockayne, D. A., Muchamuel, T., Grimaldi, J. C., Muller-Steffner, H., Randall, T. D., Lund, F. E., Murray, R., Schuber, F. & Howard, M. C. 1998. Mice deficient for the ecto-nicotinamide adenine dinucleotide glycohydrolase CD38 exhibit altered humoral immune responses. *Blood,* 92**,** 1324-33.

De Oliveira, G. C., Kanamori, K. S., Auxiliadora-Martins, M., Chini, C. C. S. & Chini, E. N. 2018. Measuring CD38 Hydrolase and Cyclase Activities: 1,N(6)-Ethenonicotinamide Adenine Dinucleotide (epsilon-NAD) and Nicotinamide Guanine Dinucleotide (NGD) Fluorescence-based Methods. *Bio Protoc,* 8**,** e2938.

Fang, F., Marangoni, R. G., Zhou, X., Yang, Y., Ye, B., Shangguang, A., Qin, W., Wang, W., Bhattacharyya, S., Wei, J., Tourtellotte, W. G. & Varga, J. 2016. Toll-like Receptor 9 Signaling Is Augmented in Systemic Sclerosis and Elicits Transforming Growth Factor beta-Dependent Fibroblast Activation. *Arthritis Rheumatol,* 68**,** 1989-2002.

Guedes, A. G. P., Paulin, J., Rivero-Nava, L., Kita, H., Lund, F. E. & Kannan, M. S. 2006. CD38-deficient mice have reduced airway hyperresponsiveness following IL-13 challenge. *American Journal of Physiology-Lung Cellular and Molecular Physiology,* 291**,** L1286-L1293.

Haffner, C. D., Becherer, J. D., Boros, E. E., Cadilla, R., Carpenter, T., Cowan, D., Deaton, D. N., Guo, Y., Harrington, W., Henke, B. R., Jeune, M. R., Kaldor, I., Milliken, N., Petrov, K. G., Preugschat, F., Schulte, C., Shearer, B. G., Shearer, T., Smalley, T. L., Jr., Stewart, E. L., Stuart, J. D. & Ulrich, J. C. 2015. Discovery, Synthesis, and Biological Evaluation of Thiazoloquin(az)olin(on)es as Potent CD38 Inhibitors. *J Med Chem,* 58**,** 3548-71.

Jablonski, K. A., Gaudet, A. D., Amici, S. A., Popovich, P. G. & Guerau-De-Arellano, M. 2016. Control of the Inflammatory Macrophage Transcriptional Signature by miR-155. *PLoS One,* 11**,** e0159724.

Johnson, M. E., Mahoney, J. M., Taroni, J., Sargent, J. L., Marmarelis, E., Wu, M. R., Varga, J., Hinchcliff, M. E. & Whitfield, M. L. 2015. Experimentally-derived fibroblast gene signatures identify molecular pathways associated with distinct subsets of systemic sclerosis patients in three independent cohorts. *PLoS One,* 10**,** e0114017.

Kanamori, K. S., De Oliveira, G. C., Auxiliadora-Martins, M., Schoon, R. A., Reid, J. M. & Chini, E. N. 2018. Two Different Methods of Quantification of Oxidized Nicotinamide Adenine Dinucleotide (NAD(+)) and Reduced Nicotinamide Adenine Dinucleotide (NADH) Intracellular Levels: Enzymatic Coupled Cycling Assay and Ultra-performance Liquid Chromatography (UPLC)-Mass Spectrometry. *Bio Protoc,* 8**,** e2937.

Misharin, A. V., Morales-Nebreda, L., Mutlu, G. M., Budinger, G. R. & Perlman, H. 2013. Flow cytometric analysis of macrophages and dendritic cell subsets in the mouse lung. *Am J Respir Cell Mol Biol,* 49**,** 503-10.

Prasad, S., Neef, T., Xu, D., Podojil, J. R., Getts, D. R., Shea, L. D. & Miller, S. D. 2018. Tolerogenic Ag-PLG nanoparticles induce tregs to suppress activated diabetogenic CD4 and CD8 T cells. *J Autoimmun,* 89**,** 112-124.

Roberson, E. D. O., Cao, L., Morales-Heil, D. J., Korman, B. & Varga, J. 2016. Biomarker Identification & Molecular Sub-Classification in Systemic Sclerosis for Precision Medicine Using RNA-Seq. *Arthritis & Rheumatology,* 68.

Sargent, J. L., Li, Z., Aliprantis, A. O., Greenblatt, M., Lemaire, R., Wu, M. H., Wei, J., Taroni, J., Harris, A., Long, K. B., Burgwin, C., Artlett, C. M., Blankenhorn, E. P., Lafyatis, R., Varga, J., Clark, S. H. & Whitfield, M. L. 2016. Identification of Optimal Mouse Models of Systemic Sclerosis by Interspecies Comparative Genomics. *Arthritis Rheumatol,* 68**,** 2003-15.

Skaug, B., Khanna, D., Swindell, W. R., Hinchcliff, M. E., Frech, T. M., Steen, V. D., Hant, F. N., Gordon, J. K., Shah, A. A., Zhu, L. S., Zheng, W. J., Browning, J. L., Barron, A. M. S., Wu, M. H., Visvanathan, S., Baum, P., Franks, J. M., Whitfield, M. L., Shanmugam, V. K., Domsic, R. T., Castelino, F. V., Bernstein, E. J., Wareing, N., Lyons, M. A., Ying, J., Charles, J., Mayes, M. D. & Assassi, S. 2020. Global skin gene expression analysis of early diffuse cutaneous systemic sclerosis shows a prominent innate and adaptive inflammatory profile. *Annals of the Rheumatic Diseases,* 79**,** 379-386.

Tarrago, M. G., Chini, C. C. S., Kanamori, K. S., Warner, G. M., Caride, A., De Oliveira, G. C., Rud, M., Samani, A., Hein, K. Z., Huang, R., Jurk, D., Cho, D. S., Boslett, J. J., Miller, J. D., Zweier, J. L., Passos, J. F., Doles, J. D., Becherer, D. J. & Chini, E. N. 2018. A Potent and Specific CD38 Inhibitor Ameliorates Age-Related Metabolic Dysfunction by Reversing Tissue NAD(+) Decline. *Cell Metab,* 27**,** 1081-1095 e10.

Yokoi, H., Kasahara, M., Mori, K., Ogawa, Y., Kuwabara, T., Imamaki, H., Kawanishi, T., Koga, K., Ishii, A., Kato, Y., Mori, K. P., Toda, N., Ohno, S., Muramatsu, H., Muramatsu, T., Sugawara, A., Mukoyama, M. & Nakao, K. 2012. Pleiotrophin triggers inflammation and increased peritoneal permeability leading to peritoneal fibrosis. *Kidney Int,* 81**,** 160-9.

Yushkevich, P. A., Piven, J., Hazlett, H. C., Smith, R. G., Ho, S., Gee, J. C. & Gerig, G. 2006. User-guided 3D active contour segmentation of anatomical structures: significantly improved efficiency and reliability. *Neuroimage,* 31**,** 1116-28.